

Republic of Iraq
Ministry of Higher Education and Scientific Research
AL- Nahrain University
College of Science
Department of physics



Multi-Temporal Analysis of Environmental Changes in Marsh Region by Landsat Images

A thesis Submitted to
the college of science AL-Nahrain University as a partial fulfillment
of the Requirement for the Degree of Master of Science
in Physics

By
Eshtar Hussain Nasser
(B.Sc. 2004)

Supervisor
Dr. Salah A. Saleh

Shawwal
November

1428 A. H.
2007 A. D.

Certification

We certify that this thesis was prepared under our supervision at the Al-Nahrain University as a partial requirement for the degree of **Master of Science in Physics**.

Signature:

Name: Dr. Salah A. Saleh

Title: Assist Professor

Address: Dept. of physics

College of Science

Al-Nahrain University

Date: / / 2007

In view of the recommendations, we present this thesis for debate by the examination committee.

Signature:

Name: Dr. Ahmad K. Ahmad

Title: (Assist Professor)

Head of Physics Department

Date: / / 2007

Examination Committee Certification

We certify that we have read the thesis entitled "*Multi-Temporal Analysis of Environmental Changes in Marsh Region by Landsat Images*" and as an examination committee, examined the student

"**Eshtar Hussain Nasser**" on its contents, and that in our opinion it is adequate for the partial fulfillment of the requirements of the degree of **Master of Science in Physics**.

Signature:

Name: **Dr. Ayad A. Al-Ani**

Title: **Assistant Professor
(Chairman)**

Date: **/11/2007**

Signature:

Name: **Dr. Abd Al-Razzak T. Ziboon**

Title: **Assistant Professor
(Member)**

Date: **/11/2007**

Signature:

Name: **Dr. Ala S. Mahdi**

Title: **Lecture
(Member)**

Date: **/11/2007**

Signature:

Name: **Dr. Salah A. Saleh**

Title: **Lecture
(Supervisor)**

Date: **/11/2007**

Approved by the College Committee of Postgraduate studies

Signature:

Name: **Dr. LAITH ABDUL AZIZ AL- ANI**

Title: **Assistant Professor
(Dean of the College of Science)**

Date: **/ /2007**



Acknowledgment

At first thanks to ALLAH for his graces that enabled me to continue the requirements of my study.

My regards and gratitude are extended to my supervisor Dr. Salah A. Saleh for his remarks and efforts and information through this work,

I am most grateful to the Dean of college of Science and Head and Staff of the department of physics at AL-Nahrain University.

I wish to thank to my parents, aunt, brothers and thank you for every one to assist through this study.

Eshar

Abstract:

Iraqi marshes were considered the largest wetland in the Middle East and characterized by varied environment (such as river, lakes and vegetation covers). During the last decades the Iraqi marshes subjected to many artificial and natural changes. These changes have impacts on its ecosystem (land cover, vegetation and aquatic environment).

The aim of this study is detect environmental changes in the Iraqi marsh for the period 1973-2004, by using multi-temporal and multi-spectral images with digital image techniques. These techniques include digital mosaic, geometric correction, image enhancement, image classification; supervised (by using maximum likelihood method) and unsupervised (by using Isodata method), Normalized Difference Vegetation Index (NDVI) for the images (1973, 1990, 2000, 2003, 2004) and computed surface radiant temperature for the images (1990, 2000, 2003, 2004).

Series of Landsat images shows that the Iraqi marshes are desiccated vegetation cover and water decrease during the period 1990- 2003. While 2003 shows reflooding the area. The results show that NDVI is good indicator for vegetation area and surface temperature. There is negative correlation between NDVI and surface temperature.

List of Contents

Chapter One : General Introduction		
1-1	General	1
1-2	Marshes	1
1-3	Effect drainage in Iraqi marshes	2
1-4	Site description for Iraqi marshes	3
1-4-1	Area and location	3
1-4-2	Climate	5
1-5	Aim of study	6
1-6	Previous studies	7
1-7	Thesis layout	11
Chapter Two : Physical Principle of Remote Sensing Technique		
2-1	Introduction	12
2-2	Fundamental of remote sensing	12
2-3	Electromagnetic energy interaction in the atmosphere	14
2-3-1	Absorption	14
2-3-2	Scattering	15
2-4	Electromagnetic energy interaction with earth feature	16
2-5	Spectral Reflectance	18
2-5-1	Spectral reflectance for water	18
2-5-2	Spectral reflectance for vegetation	18
2-5-3	Spectral reflectance for soil	20
2-6	Thermal Infrared remote sensing	20
2-7	Temperature and Emissivity	23
2-8	Interpretation of thermal IR images	24
2-9	Resolution	25
2-10	Landsat System	27
Chapter Three: Theoretical Background of Digital Image Processing		
3-1	Introduction	29
3-2	Digital image processing	29
3-2-1	Image preprocessing	30
3-2-2	Digital Image mosaic	36
3-2-3	Image enhancement	38
3-2-4	Image classification	40
3-2-4-1	Unsupervised classification	40
3-2-4-2	Supervised classification	42
3-3	Vegetation indices	46
3-4	Surface radiant temperature	48
3-5	Correlation between surface radiant temperature & NDVI	50

Chapter Four: Practical Work (Results and Discussion)		
4-1	Introduction	51
4-2	Data Acquisition	51
4-3	Digital image processing	52
4-3-1	Image digital mosaic	52
4-3-2	Geometric correction	60
4-3-3	Image enhancement	64
4-3-4	Image classification	68
4-3-4-1	Unsupervised classification	70
4-3-4-2	Supervised classification	72
4-4	Normalized Difference Vegetation Index(NDVI)	76
4-5	Surface radiant temperature	82
4-6	Correlation analysis of surface temperature and NDVI	87
Chapter Five : Conclusions and Recommendations		
5-1	Conclusions	89
5-2	Recommendations	90
References		91

List of Figures

Figure No.	Title	Page
(1-1)	Location of study area that used in this study	4
(1-2)	Temperature distribution in Fahrenheit scale	6
(2-1)	Show elements of a remote sensing system	12
(2-2)	Atmospheric windows in the electromagnetic spectrum	14
(2-3)	Interaction between electromagnetic energy and matter	16
(2-4)	Spectral reflectance curves for water, soil, and vegetation	19
(2-5)	Blackbody radiation spectral radiant exitance curves at various temperatures.	21
(2-6)	The diurnal solar cycles radiant temperature of different covers.	25
(2-7)	Landsat TM – band 1 (four types of resolution)	26
(3-1)	Residual and RMS error per point	34
(3-2)	Illustrate resampling process	36
(3-3)	Illustrate mosaic between two images	37
(3-4)	Histogram equalization	39
(3-5)	Concept parallelepiped classifier in three dimensional feature space.	43
(3-6)	Concept minimum distance to mean classifier	44
(3-7)	Concept of Maximum Likelihood classifier	46
(3-8)	linear fit to the calibration data result (relation between radiance and DN values)	49
(4-1)	Show image mosaic for image Landsat TM(7/9/1990) d6 (thermal band)	54
(4-2)	Show image mosaic for image Landsat ETM+(26/3/2000) thermal band	55
(4-3)	Image mosaic for image Landsat ETM+ (6/5/2003) band(1,2,3,4)	56
(4-4)	Show image mosaic for image Landsat ETM+ (6/5/2003) thermal band	57
(4-5)	Show image mosaic for image Landsat ETM+ (2/2/2004) band(1,2,3,4)	58
(4-6)	Show image mosaic for image Landsat ETM+ (2/2/2004) (thermal band)	59
(4-7)	Shows locations of the GCPs on the two images	62
(4-8)	Illustrate image inside the polygon represent study area (7/9/1990) band6	63
(4-9)	Show Landsat ETM+ (26/3/2000)band6 image for study area and its histogram before and after applying contrast stretching	65

(4-10)	Show Landsat ETM+ (6/5/2003)band 6 image for study area and its histogram before and after applying contrast stretching	66
(4-11)	Show Landsat ETM+(2/2/2004) band6 image for study area and its histogram before and after applying the histogram equalization	67
(4-12)	Landsat images for study area before applying classification technique	69
(4-13)	illustrate unsupervised classification of Landsat images at different times	71
(4-14)	illustrate supervised classification of Landsat images at different times by using maximum likelihood method	74
(4-15)	Shows area percentage for each class for 1973, 1990, 2000, 2003, 2004	75
(4-16)	show NDVI image for image Landsat	78
(4-17)	show NDVI images with false color	80
(4-18)	Average NDVI for land use classes	81
(4-19)	Show calculate surface temperature	83
(4-20)	Thermal images for study area	84
(4-21)	Thermal images with false color	85
(4-22)	Average temperature for land use classes	86
(4-23)	show correlation between NDVI and surface temperature	88

List of Tables

Table NO.	Title	Page
(2-1)	Sensors used on Landsat-1 to -7 missions	28
(4-1)	Illustrate data used in the study	51
(4-2)	The position of the GCPs on the input image 1973 and the reference image (2/2/2004)	61
(4-3)	Results of unsupervised classification for Landsat images by using ISodata method	72
(4-4)	show results supervised classification for Landsat images by using maximum likelihood method	74
(4-5)	Average NDVI for land use classes	80
(4-6)	Average surface temperature for land use classes	86
(4-7)	Correlation analysis of temporal surface temperature and NDVI	87

Abbreviations

DN	Digital Number
ERDAS	Earth Resource Data Analysis System
TM	Thematic Mapper
ETM	Enhanced Thematic Mapper
MSS	Multispectral Scanner
ETM+	Enhanced Thematic Mapper Plus
GCPs	Ground Control Points
RMS error	Root Mean Square error
GIS	Geographic Information System
ISODATA	Iterative Self Organizing Data Analysis
Landsat	Land Satellite
NASA	National Aeronautics and Space Administration
UNEP	United Nations Environment Programme
NDVI	Normalized Difference Vegetation Index
SR	Simple Ratio
DVI	Difference Vegetation Index
TNDVI	Transformed Normalized Difference Vegetation Index
PVI	Perpendicular Vegetation Index
SAVI	Soil Adjust Vegetation Index
BSI	Bare Soil Index
NIR	Near Infrared
Near IR	Near Infrared
TIR	Thermal Infrared
UTM	Universal Transverse Mercator
WGS 84	World Geodetic System

CHAPTER ONE
General Introduction

1-1 General

Remote sensing is defined as the technique of obtaining information about objects through the analysis of data collected by special instruments that are not in physical contact with the objects of investigation [1].

Remote sensing is an interesting and exploratory science, as it provides images of areas in a fast and cost-efficient manner, and attempts to demonstrate the "what is happening right now" in a study area.

Also remote sensing techniques give quick methods to detect the environmental changes, such that change detection is an important application of remote sensing in environmental. Change detection is a process of identifying differences in the state of objects or phenomena by observing them at different time (multi-temporal analysis)[2], therefore change detection became useful tool for detecting land cover changes. It has enabled to observe changes over large areas and provided long-term monitoring capabilities. In general digital change detection techniques using temporal remote sensing data are useful to help analyzed these data, and provided detailed information for detecting change in land cover. This modern technique used in our study. The area under study is Iraqi marshes that considerable one of the distant areas.

1-2 Marshes:

Marsh is small lakes and ponds full, yellow iris, and many other types of plant life [3]. Marshes are frequently or continually flooded wetland characterized by emergent herbaceous vegetation adapted to saturated soil conditions, changing water flows and mineral soils [4]. Marsh is one type of wetlands is not "useless swamps" as they have often been perceived, but are among the most productive ecosystems in the

world. Wetlands do much more than provide a home for wildlife. Wetlands are also natural sponges. When flood waters overflow the banks of streams and rivers the porous soils and plants of wetland soak-up tremendous amount of the excess water. Water then seeps slowly back into the stream to prevent downstream flooding. In times of drought, wetlands are fed by ground water which is released into streams to keep them flowing year round [5].

1-3 Effect drainage in Iraqi Marshes:

People lived in/around wetlands and interior of marshes, building reeds house on artificial floating island of reeds, moving around by boat, selling reed mats, and living on fish, water buffalo, and rice. Wildlife also lived in the marshes. In 1979 survey found 81 species of waterfowl, including birds which were rare or endemic. But the mid-century engineers drew up plans to drain these marshes, as wasteful evaporators of potential irrigation water. In 1970 Turkey dammed the Euphrates, reducing water to the marshes far downstream. In 1985 the Iraqi government built levees and drained part of the marshes to develop the oil field there [6].

In 1990, shortly after the Iran-Iraq war, marsh had dried out as a result of causeways constructed to ease military transport in otherwise difficult terrain [7]. The numbers of people live in marsh dwindled from roughly 400,000 in 1950 to 250,000 in 1991, so that by January 2003 the majority of the marshes became wastelands [8].

The impact of marshes desiccation on wildlife was devastating. Several endemic species of mammals, birds and fishes may have become extinct.

Fisheries in the marshlands disappeared, and Gulf fisheries dependent on the marshland habitat for spawning migrations and nursery ground, also experienced significant reductions. Ecosystem damage extended to the Shatt-al-Arab and Arabian Gulf [3]. All of these negative trends point to the inevitable demise of the marshland ecosystem within 2-3 year unless steps are taken soon to reverse the damage being done [7].

Since May 2003, rapid and significant have been in the Iraqi marshlands, water began to return to the marshlands through the actions of Iraqi's Ministry of water Resources [9].

1-4 Site description for Iraqi marshes:

1-4-1 Area and Location:

Iraqi marshes lies in the southern part of Iraq, the Iraqi marshes cut across three of Iraq's eighteen provinces: Misan (originally Al-Amarah), Dhi-Qar (originally Al-Nasiriyah), and Al-Basrah. The heartland of the marshes comprised three principal areas [10]:

1. The Al-Hammar marshes are located south of the Euphrates, extending from near Al-Nasiriyah in the west to the outskirts of Al- Basrah on the Shatt al-Arab [11].
2. The Central marshes located immediately above the confluence of the two Mesopotamian rivers, bounded by Tigris river to the east and the Euphrates river in the south, the area is roughly delimited by a triangle between Al-Nasiriyah, Qalat Saleh and Al-Qurnah[11].

3. The Al-Hawaz marsh, located east of the Tigris river and extending into Iran (where they are known as the Al-Azim marshes)[11].

The area of marshes fluctuated between 15,000 square kilometers and 20,000square kilometers [12]. Figure (1-1) show location of study area that used in this work. Locally it extends between (47.4°- 48°) longitude and (30.5°- 31.5°) latitude.

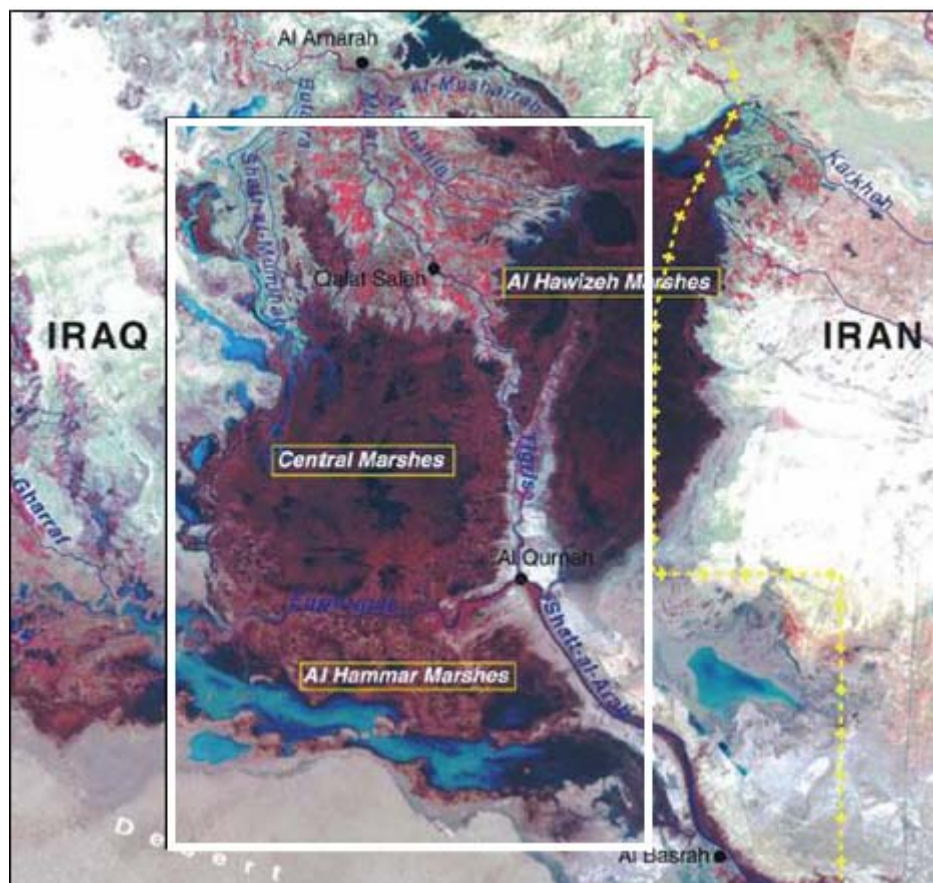


Figure (1-1) location of study area that used in this study [13]

1-4-2 Climate:

Location of marshes prevailed with desert climate that is distinguished by two clear climate seasons with short transitional durational between the dry long summer that starts from May till October and short winter that starts from December till February while spring in March and April, but autumn is represented by November[14].

The relative humidity is high and ultra values in Basrah station for weather condition range between (46-48)% in the summer and (70-75)% in the winter, the evaporation is very high from open the superficial water that is usually more than falling about (16) times. The common wind is north-west wind but the wind which brings rain blows from south to south-west, the wind speed is high during summer where it arrives it's the highest speed in June. The dust storm in winter starts from November till May while dust storms in summer starts from June till October with highest average of repetition in July[14].

During the hot, dry summers, daily marshes temperature ranged 68°F (20°C) at night to 104°F (40°C) during the day with maximum high of 122°F (50°C). In cold, wet winters, daily temperatures average from 41°F(5°C) to 59°F (15°C) with a low of 12°F(-11°C). Water temperatures in the marshes and lakes fluctuated from a low of 61°F(16°C) in the winter to high of 88°F(31°C)[12], figure (1-2) shows temperature distribution in Iraq.

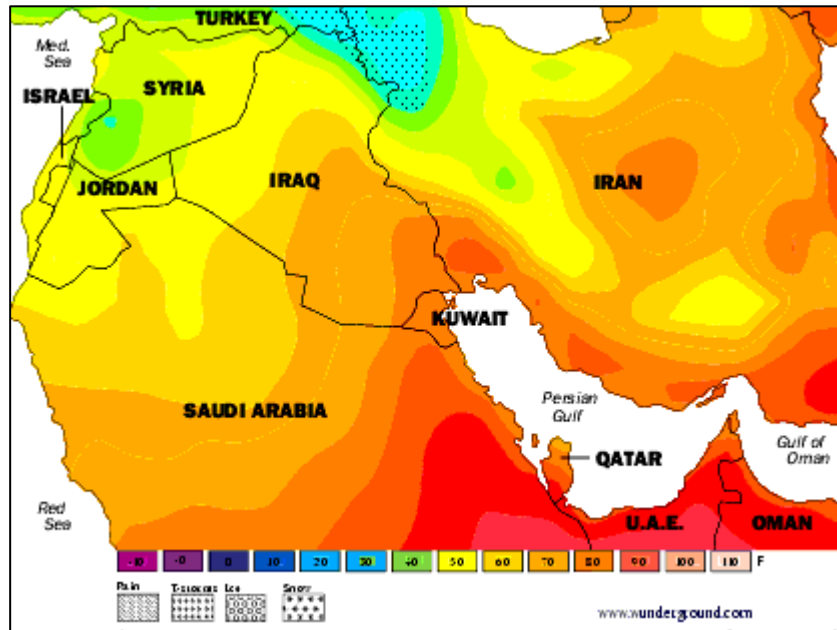


Figure (1-2) Temperature distribution in Fahrenheit scale [15]

1-5 Aim of study:

The goal of this study is detect the environmental changes in land cover/land use of Iraqi marshes areas that represent (vegetation, water, barren, and wet soil) for the period 1973-2004, using Landsat multi-temporal and multi-spectral images. Also the work aim to study impact these environmental changes on surface temperature and relation between them from through relation between normalized difference vegetation index (NDVI) and surface temperature.

1-6 previous studies:**Weng, Q. (2001) [16]**

Used techniques of remote sensing and geographic information system (GIS) to monitor and analysis urban growth patterns and effect urban growth pattern on surface temperature in Zhujiang Delta of south China. Measure the surface temperature changes from 1989 to 1997, and compute Normalized Difference vegetation index (NDVI) for 1989 and 1997. Conclude that the remote sensing technique and GIS are effective in monitoring and analyzing urban growth patterns and in evaluating urbanization impact temperature.

Ping, p. & et al (2001) [17]

Used of Landsat 7 ETM+ data for indicating temperature difference in urban areas, at Singapore and part of Johor of Malaysia and compare the relation between urban temperature and land cover types. This study shows that the temperature of various land cover types was distributed from low in sea surface water, inland water, forest grass, to high in barren land, high building, residential area, industrial area. Demonstrate the usefulness Landsat ETM+ data for mapping the thermal pattern distribution which can be used as the reference for urban planning.

Zhou, L. & et al (2003) [18]

Analyzed the relation between satellite- based measures vegetation greenness and climate by land cover type through 1982 and 1999. Estimated statistically meaningful relation between NDVI and climate during spring, summer and autumn for all forest land cover types in the north of America and Eurasia.

Akkartal, A. & etal (2004) [19]

Changes vegetation biomass in some region of Turkey (Luleburgaz district, Krklareli, Thrace) for period (1987-2003) was analyzed by using three multi-temporal Landsat TM scenes (1987, 1993, 2000) and one Spot Xp scene (2003); and by used five different types of vegetation indices included Simple Ratio (SR), Difference Vegetation Index (DVI), Normalized Difference Vegetation Index (NDVI), Transformed Normalized Difference Vegetation Index (TNDVI), Perpendicular Vegetation Index (PVI). This study shows that the multi-temporal and multi-sensor satellite data have a great success in vegetation biomass analysis.

Andy,Y.K & Christopher.S(2004) [20]

Comparative analysis of thermal environments in New York city and Kuwait city by using Landsat ETM+ band 6 thermal. This study shows that surface temperature is highly sensitive to vegetation as well as surface soil moisture content, that demonstrate most successful applications of remote sensing to the urban environment generally involve measurement of physical quantities related to environmental conditions such as surface temperature and vegetation abundance.

Riadh K. A. (2005) [2]

Studied change detection of environmental system using satellite images in Shatt Al-Arab region and part of Hawr Al-Hammar during 30 years through the comparative of different Landsat images, and concluded the images taken by satellite revealed its importance and economical values for frequent monitoring of environmental changes of large areas and represents a liable information archives through which historical changes of the study area can be detected.

UNEP (2005) [21]

Monitoring reflooding and vegetation changes in Iraq marshes for the last years (2004-2005) depending on average values of the NDVI are calculated in various areas representing different land cover types (desert, vegetation, water). This study shows that in water and desert $NDVI < 0.125$ and vegetation > 0.125 in 2005, and show that evaluation of the three main marsh by compared the areas for years 1973, 2004, 2005, results the marsh area in 2000 (almost complete desiccation) is 15%, in year 2004%, in year 2005 is 42%.

Myung H. J. & et al (2006) [22]

Analyze the pattern of the land cover change, surface temperature as well as NDVI distribution in the agriculture area for Ansong-Watershed area of Korea using multi-temporal of Landsat satellite image (1987, 1993, 2000) and GIS technique; so that classified this area in to 6 classes included forest, paddy field, field, stream, urban, barren; by maximum likelihood method of the supervised classification, in addition produced NDVI and surface temperature. This study shows that surface temperature high in 1993 compare with 1987 due to decrease forest area, paddy field and increase barren area and urban and industrial zones, also shows that when the large population, temperature id high and NDVI is low due to correlation between temperature and NDVI is negative.

Ali K. S., (2006) [3]

Applied remote sensing techniques and GIS to study the water quality in the Iraq marshes through test and analyze samples of water feeding the marsh as well as samples of marsh water. In this study conducted of spectral reflection polluted water in the laboratory by spectral bands

which imitate those used in the detectors of Landsat TM and try to evaluate the suspended reflection and choose the best spectral reflection and concentrations of polluted materials.

Aseel A. S., (2006) [23]

Utilized remote sensing and GIS techniques for description of Al-Hammar marsh by produce a digital soil map which contains land cover, soil classification and some of chemical properties which mostly affect the spectral behavior of soil and the nature of the soil of Al-Hammar marsh. This study shows that the selected visible bands in the digital visual interpretation process are considered an optimum to sense the soil types.

Emzahim A. A., (2006) [24]

Used remote sensing and GIS techniques to evaluate environment of marshes zone. This study shows new remote sensing technique for evaluation of the structure member for constructing low cost housing in south of Iraqi marshes. Also this study describes water, soil properties and temporal changes in this region for the period 1973- 2004 years.

1-7 Thesis layouts

In addition to this chapter this thesis consists of four chapters outlined below.

Chapter two: will be dedicated to explain the physical principle of remote sensing technique.

Chapter three: Illustrates the theoretical back ground of digital image processing and the theoretical of some indicators used to evaluate environment of study region represent NDVI and surface radiant temperature.

Chapter four: Illustrates the results and discussion obtained from practical work.

Chapter five: Summarized conclusions and recommendations for future studies.

CHAPTER TWO

Physical Principle of Remote Sensing Technique

2-1 Introduction

The principles of remote sensing are based primarily on the properties of the electromagnetic spectrum and the geometry of airborne or satellite platforms relative to their targets. This chapter includes fundamentals of remote sensing and discusses remote sensing process, electromagnetic interaction with the atmosphere and earth surface, physical principle of thermal infrared remote sensing thermal infrared.

2-2 Fundamentals of remote sensing:

Remote sensing is the art and science involving the detection, identification, classification, delineation, and analysis of earth surface features and phenomena using imagery acquired from terrestrial, air craft, and satellite platforms equipped with photographic and non-photographic sensors using visual computer assisted interpretation [25]. The process of remote sensing involves the detection and measurement of different wavelengths reflected or emitted from distant objects or materials so that all remote sensing imaging systems have the following elements[26], as shows figure (2-1).

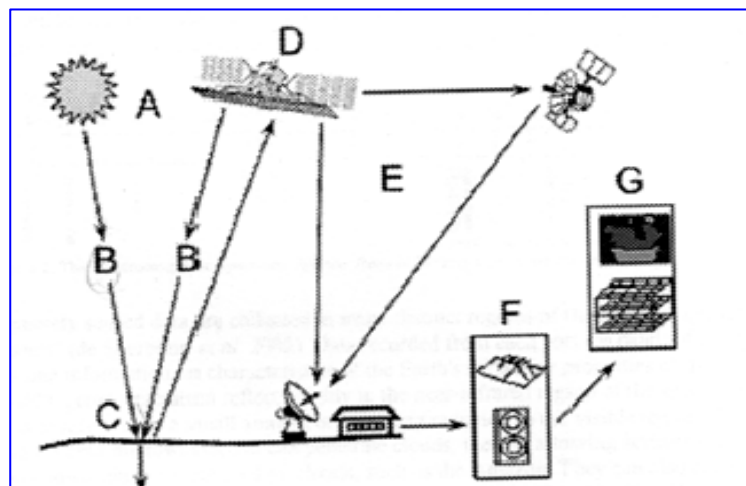


Figure (2-1) Show elements of a remote sensing system[26]

1- Energy source or illumination (A):

A basic requirement for remote sensing is an energy source to illuminate or provide electromagnetic energy to the target of interest. The source energy utilized for remote sensing observation is used to divide remote sensing into passive and active system.

2- Radiation and the Atmosphere (B):

As the energy travels from its source to the targets, it will come in contact and interact with the atmosphere it passes through. This energy travels from the target to the sensor.

3- Interaction with the target (c):

Once the energy makes its way to the target through the atmosphere, it interacts with the target depend on properties of the both the target and the radiation.

4- Recording of energy by the sensor (D):

After the energy has been scattered by, or emitted from the target, a sensor collects and records the electromagnetic radiation (EMR).

5- Transmission, Reception and processing (E)

The energy recorded by the sensor has to be transmitted, often in electronic form, to a receiving and processing station where the data are processed into an image.

6- Interpretation and Analysis (F):

The processed image is interpreted, visually or digitally/electronically, to extract information about the target.

7- Application (G):

The final element of the remote sensing process is achieved by applying the information that has been extracted from the imagery about the target in order to better understand it, reveal some new information, or assist in solving a particular problem.

2-3 Electromagnetic Energy Interaction in the Atmosphere:

Electromagnetic energy emitted by the sun must pass through the atmosphere before it reaches the surface of the earth. A sensor on board a satellite or aircraft measures reflected radiation which also has pass the atmosphere or at least a part of the atmosphere. The atmosphere affects to the energy radiation passes through it, so that this radiation interacts with the constituent gases of the atmosphere; causing change of the electromagnetic energy by absorption and scattering energy:

2-3-1 Absorption:

Among the numerous gases of the atmosphere, the most significant absorbers of EM energy are oxygen (O_2), nitrogen (N_2), ozone (O_3), carbon dioxide (CO_2); and water (H_2O). The atmosphere's gases are selective absorbers to wavelength [1].

Figure (2-2) shows major spectral regions pertinent to remote sensing, showing atmospheric windows (white) and (black) the gases responsible for absorption.

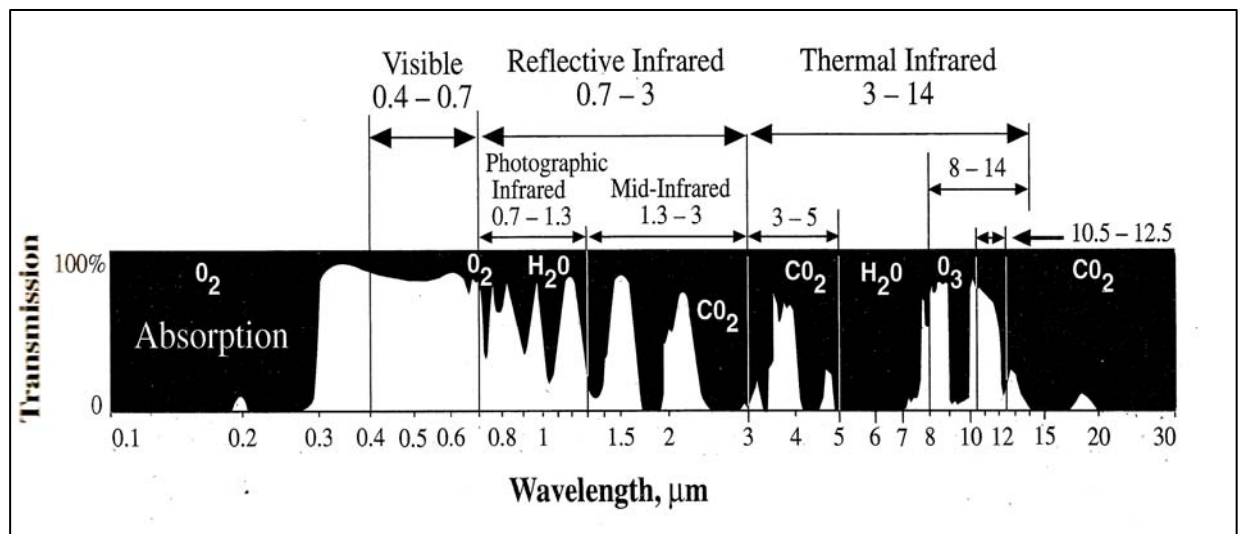


Figure (2-2) Atmospheric windows in the electromagnetic spectrum[27]

2-3-2 Scattering:

Atmosphere scattering results from interactions between radiation and gases and particles in the atmosphere. Two types of scattering are recognized; selective scattering and non-selective scattering

A-Selective scattering: is two types

- **Rayleigh scatter:**

Rayleigh scattering or molecular scattering occurs when the dimensions of the scatters are small compared with the wavelengths of the electromagnetic radiation. The amount of scattering is inversely proportional to the fourth power of the wavelength. Within the visible range of the electromagnetic spectrum, blue light is scattered much greater degree than green or red [28].

- **Mie scatter:**

Mie scattering or non-molecular scattering occurs when of the aerosols in the atmosphere are approximately the same as the wavelengths of the electromagnetic radiation [28] .

Mie scattering is also wavelength dependent and varies approximately as the inverse the wavelength [28]. Therefore Mie scattering influences long radiation wavelength than Rayleigh scattering

B-Non- Selective Scattering:

Non- selective scattering becomes operative when the lower atmosphere, so that scattering at all wavelengths occurs equally with aerosols dimensions are greater than approximately ten times the wavelength of the radiation[1].

2-4 Electromagnetic Energy Interaction with Earth Surface

Feature:[1]

Objects sensed interact differently to incident energy according to their physical or chemical properties. Depending to their specific features and behavior with regard to different wavelengths, objects can be recognized on remote sensing data. When EMR strikes a surface, it may be reflected, scattered, absorbed or transmitted as show in figure (2-3).

-Transmission is the process by which incident radiation passes through object without measurable attenuation; the substance (object) is thus transparent to the radiation for example (water and air).

-Reflection (also called specular reflection) describes the process where by incident radiation bounces off the surface of the substance in a single, predictable direction. The angle of reflection is always equal and opposite to the angle of incidence. Specular reflection causes no change to either EMR velocity or wavelength.

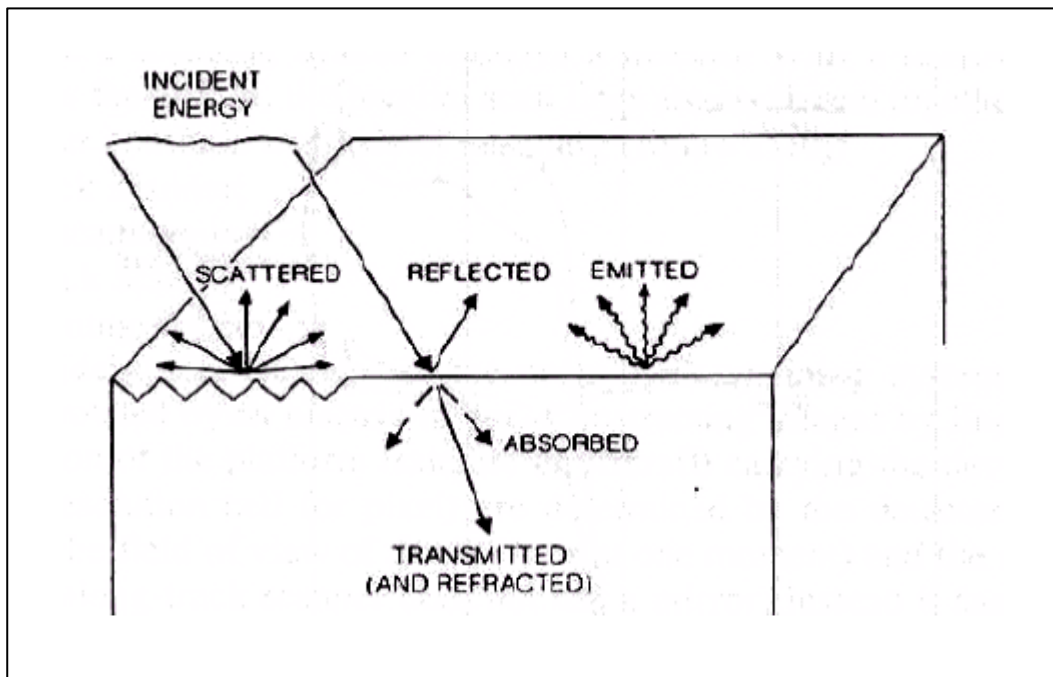


Figure (2-3) Interaction between electromagnetic energy and matter[29].

-Scattering (also called diffuse reflection) occurs when incident radiation is dispersed or spread out unpredictably in many different directions. The scattering process occurs with the surfaces that rough relative to the wavelengths of incident radiation, such surfaces are called diffuse reflectors. EMR velocity and wavelength are not affected by scattering process.

-Absorption is the process by which incident radiation is taken in by the medium. For this to occur the substance must be opaque to the incident radiation. A portion of the absorbed radiation is converted into internal heat energy, which is subsequently emitted or reradiated at longer thermal infrared. The interrelationships between energy interactions, as a function of wavelength (λ) can be expressed in the following manner [1]:

$$E_I(\lambda) = E_T(\lambda) + E_R(\lambda) + E_A(\lambda) \quad \dots\dots\dots(2-1)$$

Where

$E_I(\lambda)$ = incident radiant energy

$E_T(\lambda)$ = decimal fraction transmitted

$E_R(\lambda)$ = decimal fraction reflected (specular and diffuse)

$E_A(\lambda)$ = decimal fraction absorbed

Most opaque materials transmit no incident energy, hence $E_T(\lambda)=0$ and equation(2-1)becomes:

$$E_R(\lambda) + E_A(\lambda) = 1 = E_I(\lambda) \quad \dots\dots\dots(2-2)$$

Equation (2-2) indicate when object has high reflectance value; low absorption value, but when high absorption value and minimal reflection value due to only the part of incident radiation that is absorbed by an object is effective in heating it, causes high temperature.

2-5 Spectral Reflectance:

The physical and chemical characteristics of materials define their reflectance and emittance spectra that can be used identify them. The spectral reflectance refers to the ratio of object radiant energy reflected to that incident on object. Identification of many earth surface features are primarily a function of the spectral response of those features [30].

The spectral characteristics of various earth surface features do not remain constant; they change with geographic location and time. Temporal change in spectral response can either natural or caused by human beings. Remote sensing change detection techniques can be used to monitor these temporal changes. Figure (2-4) illustrate the spectral reflectance curves of water, vegetation, soil.

2-5-1 Spectral Reflectance for Water:

The reflectance of clear water is generally low. However the reflectance is high at blue end the spectrum and decrease as wavelength increase. Hence, water appears dark bluish to the visible eye. Turbid water has some sediment suspension that increases the reflectance in the red end of the spectrum would be brownish in appearance [31].

2-5-2 Spectral Reflectance for Vegetation:

Spectral reflectance of vegetation depends on the properties of the leaf are including [28]:

- 1- leaf pigmentation (chlorophyll)
- 2- leaf thickness and composition
- 3- Amount of water in the leaf tissue

In the visible portion of the spectrum, the reflection from blue and red is low because the absorption by chlorophyll for photosynthesis where the high reflectance in green part [28]. In the near-infrared (NIR) region, the reflectance is much higher than that in visible band due to cellular structure in the leaf. The reflectance curves can be used for identification of vegetation type. For example, the reflectance spectra of dry grass and green grass can be distinguished; so that the reflectance of green grass has high reflectance in near-infrared region and low reflectance in visible region, but dry grass has higher reflectance in visible region and lower reflectance in the near-infrared region because of no chlorophyll [31].

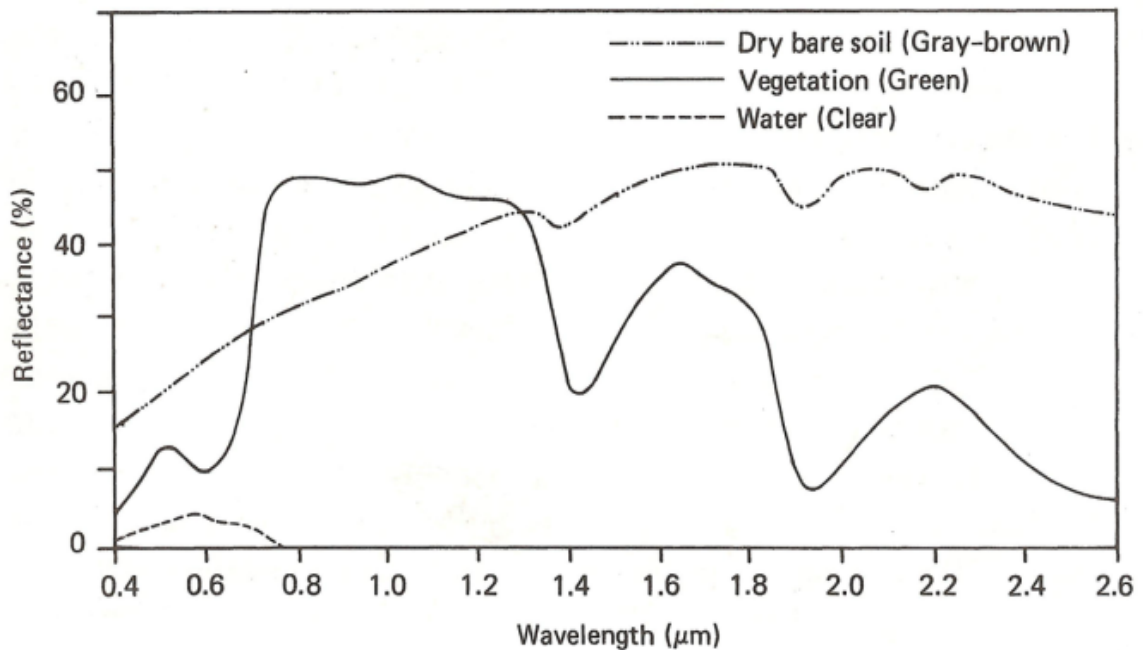


Figure (2-4) spectral reflectance curves for water, soil, and vegetation [30]

2-5-3 Spectral Reflectance for Soil:

Spectral reflectance of soil generally increases with increasing wavelength. The soil is a complex mixture of materials having various physical and chemical properties which can affect the spectral reflectance of soil, therefore spectral reflectance depending on [28]:

- 1- soil texture (presence of sand, silt, and clay) and moisture content
- 2- organic matter content
- 3- iron-oxide content
- 4- surface roughness

2-6 Thermal Infrared Remote Sensing:

Thermal radiation results from random atomic and molecular motions and is emitted by all substances having a temperature above zero (0 K, -273.16°C)[1]. This thermal radiation describes some scientists such as Planck, Stefan-Boltzmann, Wien, Kirchhoff.

Planck's radiation law related the spectral characteristics and magnitude of the emission to the temperature of the emitting body; the expression for a theoretically perfect emitter or blackbody at any given wavelength [1].

$$E_{\lambda} = C_1 / \lambda^5 [\text{EXP} (C_2/\lambda T) - 1] \dots\dots\dots(2-3)$$

Where

E_{λ} = spectral emission(spectral radiant exitance) in $\text{W}/(\text{m}^2 \cdot \mu\text{m})$.

C_1 =first radiation constant= $2\pi^5 h^6 C^3 / 15 \text{m}^3 = 3.7418 \times 10^{-6} \text{ Wm}^2$ (h =Planck's constant= $6.626 \times 10^{-34} \text{ J}\cdot\text{sec}$, and C is the light velocity)

$C_2 =$ second radiation constant $= 1.44 \times 10^2 \text{ m.K} = h c/k$ (k is the Boltzmann's constant $= 1.38 \times 10^{-23} \text{ J.K}^{-1}$).

$T =$ absolute temperature (K)

Equation (2-3) indicates that any given wavelength, the total energy of emitted blackbody radiation increases as temperature increase. It also indicates that the intensity distribution of the radiation varies with wavelength at a given temperature. So that values for E_λ are commonly used to construct energy distribution curves for objects at various temperatures (figure (2-5))

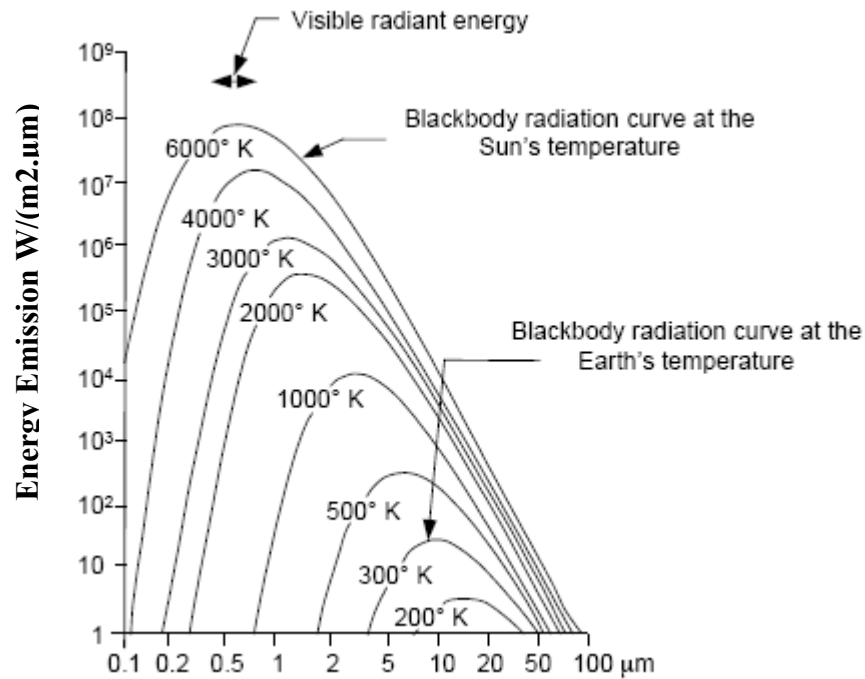


Figure (2-5) Blackbody radiation spectral radiant exitance curves at various temperatures[32].

The magnitude of radiation emitted from a blackbody over entire spectrum (area under the curve in figure (2-5)) is explained by the Stefan-Boltzmann law [1] :

$$E_{bb} = \sigma T^4 \quad \dots\dots\dots (2-4)$$

Where E_{bb} = radiant emittance from a blackbody in w/m^2

$\sigma = 5.67 \times 10^{-8} w / (m^2.K^4)$ (Stefan-Boltzmann constant)

T = absolute temperature (K)

Equation (2-4) shows that the total energy emitted from a blackbody overall wavelengths, is directly proportional to the fourth power of its absolute temperature. For example if the temperature of blackbody is raised from 300K to 600K, its temperature is doubled; but the radiant emittance increases 2^4 , or 16 times.

Wien's displacement identifies the wavelength at which the maximum amount of energy is radiated (λ_{max}) from a blackbody [1]

$$\lambda_{max} = W / T \dots\dots\dots(2-5)$$

Where $W = 2897 \mu m.K$ (Wien's constant)

T = absolute temperature (K)

Wien's displacement law shows that wavelength of maximum energy emission is inversely proportional to the absolute temperature of the blackbody. Thus, as temperature increase, λ_{max} shifts to progressively shorter wavelengths.

Also Wien's displacement identifies the atmospheric windows to use for remote sensing thermal IR emission. For example, the radiant power peak for very hot targets such as sun is within or close to the 3-to-5 μm window (figure (2-5)). The 8-to-14 μm window contains the radiant power peaks for most of the earth's passive features. Since their temperatures are in the neighborhood of 300K. For this reason, most thermal IR surveys are performed (8-14) μm .

2-7 Temperature and Emissivity(ϵ):

The temperature of an object is obtained by placing a thermometer in direct contact with an object at the same times as a remote sensing radiometer measures the temperature of the same object. The two results would be different [28].

The radiometer measures what is known as the radiant temperature T_{rad} of the body; where as the thermometer in direct contact measures the kinetic temperature T_{kin} of the body [28]. The kinetic energy of the particles of the body as that random motion causes particles to collide, resulting in changes of energy state (electron) and the emission of electromagnetic radiation. The concentration of the radiant flux of an object is the radiant temperature. Kinetic temperature and radiant temperature are not the same. The radiant temperature is always less than the kinetic temperature because objects do not behave like blackbodies and do not completely obey the Stefan-Boltzman equation. This property of objects is called emissivity(ϵ) and is defined as the ratio between the radiant flux of the object and the radiant flux of a blackbody with the same (kinetic) temperature [29]. The radiant temperature of an object is related to its kinetic temperature by the following [1]:

$$T_{\text{(radiant)}} = \epsilon^{1/4} T_{\text{(kinetic)}} \dots \dots \dots (2-6)$$

Given a constant T_{kin} , equation (2-6) shows that T_{rad} . Varies directly with ϵ .

2-8 Interpretation of Thermal IR Images:

Thermal IR images depict radiant temperature contrasts of a given ground area a toned variations. Lighter tones represent warm features, and darker tones represent cooler features. The following descriptions provide a set of general guidelines for interpreting thermal image [1]:

- 1- **Water versus soil and rock:** water is generally cooler (dark tone) than soil and rock during the day, but surface temperature are reversed at night with being the warmest (lighter tones). Because the water has thermal capacity higher than soil and rocks.

- 2- **Vegetation:** tree leaves normally appears cool (dark tones) during daylight and warm (light tones) at night. Because of vegetation transpiration is at its maximum during the day, and this process lowers leaf temperature. This type of vegetation appears warm in night time because of high water content of the leaves.

- 3- **Damp Ground:** damp ground is cooler (darker tones) than dry ground during both day and night because of evaporative cooling of contained moisture.

- 4- **Clouds and fog:** an image will depict cloud tops and fog as cold materials (dark tones) because of cloud and fog usually completely mask thermal IR emission.

The typical diurnal temperature variations for soil and, rock, water, vegetation, moist soil, and metal objects are show in figure (2-6). If all of these curves lie exactly on top of one another, then remote sensing in thermal infrared portion of the spectrum would be of no value because all the features would have the same apparent radiant temperature. There would be no contrast in the imagery between different features. There are

only two times during the day (after sunrise and near sunset) when some materials have exactly the same radiant temperature. During this crossover time period it is generally not wise to acquire thermal infrared remotely sensed data [28].

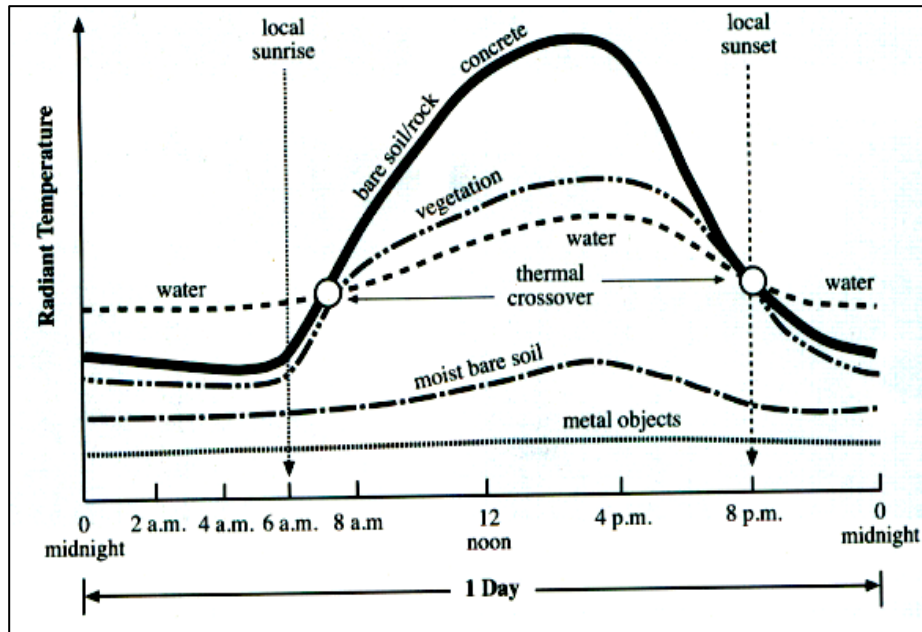


Figure (2-6) The diurnal solar cycles radiant temperature of different covers [27].

2-9 Resolution of Satellite Sensor:

Resolution is the smallest distance between two features, so that the two features can still be distinguished from each other. However, in remote sensing four types of resolution [28]:-

1-Spectral resolution:

Spectral resolution refers to the dimension and number of specific wavelength interval in the electromagnetic spectrum to which a sensor is sensitive.

2- Spatial resolution:

A measure of the amount of detail that can be observed on an image, so that two images have the same scale and for the same area. The image that shows finer details may be said to have a better spatial resolution [28].

3- Temporal resolution:

The temporal resolution of remote sensing system is measure of how often data are obtained for the same area [28].

4- Radiometric resolution:

The radiometric resolution of remote sensing is a measure of how many gray levels are measured between pure black (which could represent no reflectance from the surface) and pure white [28]. In other meaning its defines the sensitivity of a detector to differences in signal strength as it record the radiant flux reflected or emitted from the surface. Figure (2-7) illustrate four types resolution.

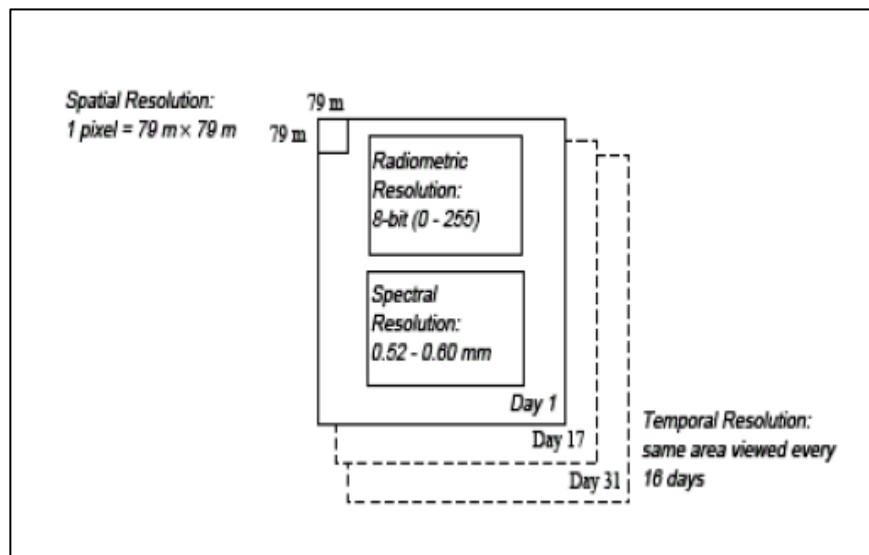


Figure (2-7) Landsat TM – band 1 (four types of resolution) [33]

2-10 Landsat System:

The first satellite in the series, for monitoring and earth observation initially named as ERTS-1 (Earth Resources Technology Satellite), which recently renamed Landsat.

Landsat-1 was launched in 1972, and then launched Landsat -2-3 in 1975 and 1978, after that was launched Landsat -4-5 in 1981-1984[34].

The Landsat series satellites has been the most successful to date, providing world wide coverage for 30 years. However, there have been failures. Landsat-1 system Failed. The greatest loss (up to date) for the Landsat series was the disappearance of Landsat-6 soon after its launched in 1993. This was to have capabilities similar to that Landsat-5, but include an Enhanced Thematic Mapper which was to obtain panchromatic (pan.) single band data (0.5- 0.9 μ m) with a resolution (spatial resolution) is 15m. Landsat-7, which was successfully launched in April 1999[35].

Landsat-1 through-7, systems have been included five different types of sensors there are:

1- Return Beam Vidicon(RBV) : is three television cameras system are sensitive to scene radiance in wavelengths from (0.48 – 0.83 μ m)

2- Multi-Spectral Scanner (MSS) has four bands which are sensitive to radiance in wavelength from (0.5 -1.1 μ m)

3- Thematic Mapper (TM) : has seven bands from visible blue, through the mid-IR, into the thermal IR portion of the electromagnetic spectrum. The TM sensor has a spatial resolution of 30m for the visible, near IR, and mid-IR wavelengths and a spatial resolution of 120m for the thermal IR band.

4- Enhanced Thematic Mapper (ETM) has same bands in (TM) sensor, plus pan. Band (0.5-0.9 μ m) has spatial resolution 15m.

5- Enhanced Thematic Mapper Plus (ETM+) has same TM bands sensor, plus pan. band (0.5-0.9 μ m) with spatial resolution 15m. Spatial resolution of ETM+ in thermal band differ from spatial resolution in TM in the thermal band, so that ETM+ has spatial resolution in thermal band is 60m. Table (2-1) illustrate sensors used on Landsat-1-7

Table (2-1) Sensors used on Landsat-1 to -7 missions [30]

sensor	Mission	Band	Sensitivity(μ m)	Resolution(m)
RBV	1,2		0.475 - 0.575	80
			0.580 - 0.680	80
			0.690 - 0.750	80
	3		0.505 - 0.750	30
MSS	1-5		0.5 - 0.6	79/82 ^a
			0.6 - 0.7	79/82 ^a
			0.7 - 0.8	79/82 ^a
			0.8 - 1.1	79/82 ^a
	3		10.4 - 12.6 ^b	240
TM	4,5	1	0.45 - 0.60	30
		2	0.52 - 0.60	30
		3	0.63 - 0.69	30
		4	0.76 - 0.90	30
		5	1.55 - 1.57	30
		6	10.4-12.5	120
		7	2.08 - 2.35	30
ETM^c	6		Above TM bands	30(120m thermal bands)
			Plus 0.5-0.90	15
ETM+	7		Above Tm bands	30 (60m thermal band)
			Plus 0.50-0.90	15

^a79m for Landsat -1 to-3 and 82m for Landsat-4-5

^b failed shortly after launched (band 8 of Landsat-3)

^c Landsat-6 launched failure

CHAPTER THREE

Theoretical Background of Digital Image Processing

3-1 Introduction:

This chapter describes the theoretical back ground of digital image processing and discusses the theoretical back ground of some indicators used to detect environmental changes of study area. These indicators consist of Normalized Difference Vegetation Index (NDVI) and surface temperature and relation between them.

3-2 Digital Image Processing:

Digital image processing involves the manipulation interpretation of digital images with the aid of computer. A digital image is represent some portion of electromagnetic spectrum is a numerical ground resolution cells. In physical form, a digital image is a two dimensional array of a small area called pixels, so that numerical representation is in the form of positive integers that are referred to a digital numbers denoted by DN [1]. The minimum DN value means no energy reflected or emitted from the scene, while maximum value often (255) for 8-bit image indicated the saturation energy received from the scene. The main processes used to apply the digital image processing are:

- 1- Image preprocessing
- 2- Image mosaic
- 3- Image enhancement
- 4- Image classification

3-2-1 Image Preprocessing:

Remote sensing system gathered data in many forms and techniques. In all these systems there are numerous errors associated with gathered data [36], such that many enhancement and classification operations will emphasize image imperfections to such an extent that useful information can be obscured [1]. Therefore, it is necessary to preprocess the remotely sensed data prior to analysis it in order to remove these errors. Hence, preprocessing is concerned with correcting a degraded digital image to its intended form.

Errors in remotely sensed data categorized as "Radiometric" and "Geometric". There are the most commonly types of error encountered in remotely sensed imagery.

- **Radiometric Correction:**

This correction is concerned with removal of distortions in the amount electromagnetic energy received by the satellite, so that this energy received is the true reflected or emitted by the surface. This kind of correction is needed because of attenuation of energy before reaches the sensor, because of sensor irregularities such as striping scan line dropping and random noise [37].

- **Geometric Correction:**

The earth rotation, earth curvature, remotely sensed instruments are not constant. These effects and other effects are influenced on extracted image and cause geometric distortions in the image, so that digital values of pixels are not represented exactly reflected and emitted energy, furthermore locations earth phenomena in photo image not

related in their locations in the nature. Therefore, should be use geometric correction process.

Geometric correction is removal distortions in the shape of the image due to sensor-earth geometry variations. Numerous systematic and non-systematic geometric distortions are inherent in raw digital images [1].

Because systematic distortions are constant over time, they are predictable, and geometric transformations are relatively simple to design and inexpensive to run [1].

Altitude and attitude variations (rolls, pitch, yaw) and topographic elevation difference are responsible for non-systematic (random) distortions in digital image [1]. These distortions more difficult more than systematic distortions, so that the removal these distortions required detailed information the image an area (ground control points GCPs), [36]. The term registration and rectification are used to describe geometric transformation [38]. The image registration is considered as an essential and important in any remote sensing analysis[36], so that registration is process of making an image conform to another image, a map coordinate system is not necessarily involved[39]. Rectifying or registering image data involves general steps [33]:

- A- Select ground control points GCPs
- B- Compute transformation
- C- Compute root mean square errors(RMS error)
- D- Resampling methods

A- Ground Control Points (GCP) Selection:

GCPs a specific pixel on an image or location on map whose geographic coordinates are known. GCPs are used to correct geometric distortions in an image by matching image coordinates(distorted) with map coordinates (rectification), or matching image coordinates (distorted) with another image coordinates (registration)[39]. GCPs are features located in the input and reference image, and GCPs select sharp features such that (main roads, river boundary, rail way line or any feature that can distinguish it in the image and map)

B- Transformation:

The most commonly used registration model uses polynomial equations, because the polynomial equations are used to convert source (input) coordinates to registered reference coordinates. Depending upon the distortion in the imagery, the number of GCPs used, and their locations relative to one another, complex polynomial equations may be required to express the needed transformation [36]. The degree of complexity of the polynomial is expressed as the order of the polynomial. The order of transformation is the order polynomial used in the transformation, usually 1st-order or 2nd-order polynomials are used.

Such that 1st-order polynomial equation is given by [33]:

$$\begin{array}{l} X_o = a_0 + a_1 x + a_2 y \\ Y_o = b_0 + b_1 x + b_2 y \end{array} \quad \left| \begin{array}{l} \dots\dots\dots(3-1) \end{array} \right.$$

Where x and y are source coordinate (input)

X_o and Y_o are rectified or registered coordinates (output)

The transformation matrix for 1st- order transformation consists of six coefficient- three for each coordinate (x, y),[33]

$$a_0 \quad a_1 \quad a_2$$

$$b_0 \quad b_1 \quad b_2$$

In order to determine the coefficients of transformation matrix, must substituted values X_o , Y_o , x , y coordinates from each GCP. The aim calculating coefficients of transformation matrix are to derive the polynomial equations for which there is the least possible amount of error when they are used to transform the reference coordinates of the GCPs into the source coordinates (input). It is not always possible to derive coefficients that produce without errors. These errors will appear because of poor positional of mouse pointer in an image and by inaccurate measurement of coordinates in image.

C- RMS error:

RMS error is the distance between the input (source) location of a GCP and the retransformed location for the same GCP. In other words, it is the difference between the desired output coordinate for a GCP and the actual output coordinate for the same point, when the point is transformed with the geometric transformation [33].

RMS error is calculated with a distance equation[33]:

$$\text{RMS error} = \sqrt{(x_r - x_i)^2 + (y_r - y_i)^2} \quad \dots\dots\dots(3-2)$$

Where x_i and y_i are input source coordinates

X_r and y_r are the retransformed coordinate

RMS error is expressed as a distance in the source coordinate system.

Residuals are the distances between the source and retransformed

coordinates in one direction. The x residual is the distance between the source x coordinate and the transformed x coordinate. The y residual is the distance between the source y coordinate and the retransformed y coordinate, (as shows in figure (3-1)), then can be expressed RMS error in this equation[33]:

$$\text{RMS error} = \sqrt{(\text{residual } x)^2 + (\text{residual } y)^2} \quad \dots\dots\dots (3-3)$$

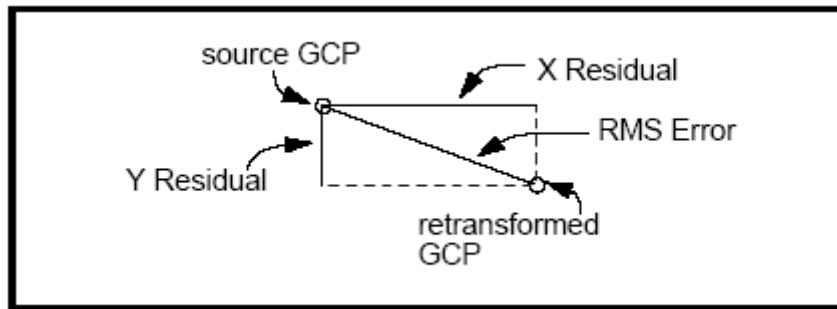


Figure (3-1) Residual and RMS error per point[33]

D- Resampling:

Resampling is process to determine the new digital number value for each of the pixel in the new transformed image. The transformation equation that was calculated to locate the GCPs in the new image is inverted so that an original value for each pixel in the new image can be determined [2], as shows (3-2) illustrates resampling process.

There are many resampling method like:

- Nearest Neighbors
- Bilinear interpolation
- Cubic convolution

● **Nearest Neighbors resampling:**

In nearest neighbors resampling the closet neighbor is chosen as the value for the image value. Analysts always used nearest neighbors resampling method because the easiest of the three methods to compute and fastest to use. Transfers original data values without averaging them as the other method do, therefore, the extremes and subtleties of the data values are not lost. This is important consideration when discriminating between vegetation types, locating an edge associated with a lineament, or determining different levels of turbidity or temperatures in a lake [33]

● **Bilinear interpolation:**

In this method takes a weighted average of four pixels in the original image nearest to the new pixel location. The averaging process alters the original pixel values and creates entirely new digital values in the output image [39].

● **Cubic convolution:**

This method goes even further to calculate a distance weighted average of a block of sixteen pixels (4×4 array) from the original image, which surround the new output pixel location [39].

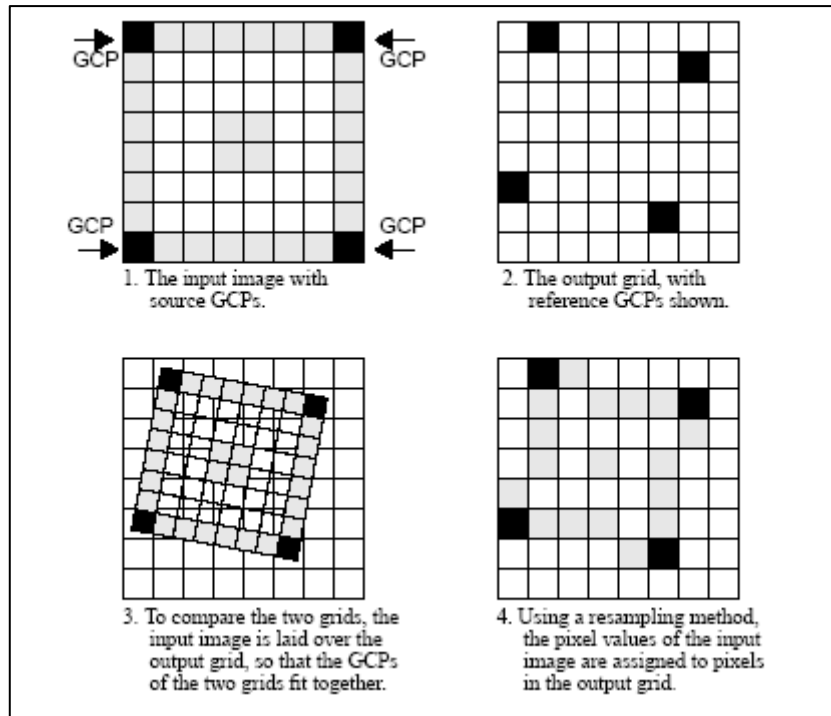


Figure (3-2) Illustrate resampling process[33]

3-2-2 Digital Image Mosaic:

Mosaic means gathering of interfered images to produce new image, as shows (3-3) illustrate the interfered between two images. The mosaic image can give a general view of entire region that is covered by the images. Mosaic image may be helpful in interpretation and producing typical maps of large area, in the past, mosaic had been done by manually. Today the digital processing provided automate mechanism in producing mosaic without wasting time and effort.

Image mosaic problem is produced non-homogeneous images because geometric correction is run of each digital image (these interfered between them to produce new images), so that appear non-homogeneous because transformation equations computed of each image caused by

distortion in mosaic image. Also extracted images at different time effected in mosaic image due to brightness different between two images and different in appearance nature earth target. Therefore mosaic image needed enhancement process to remove brightness different in images.

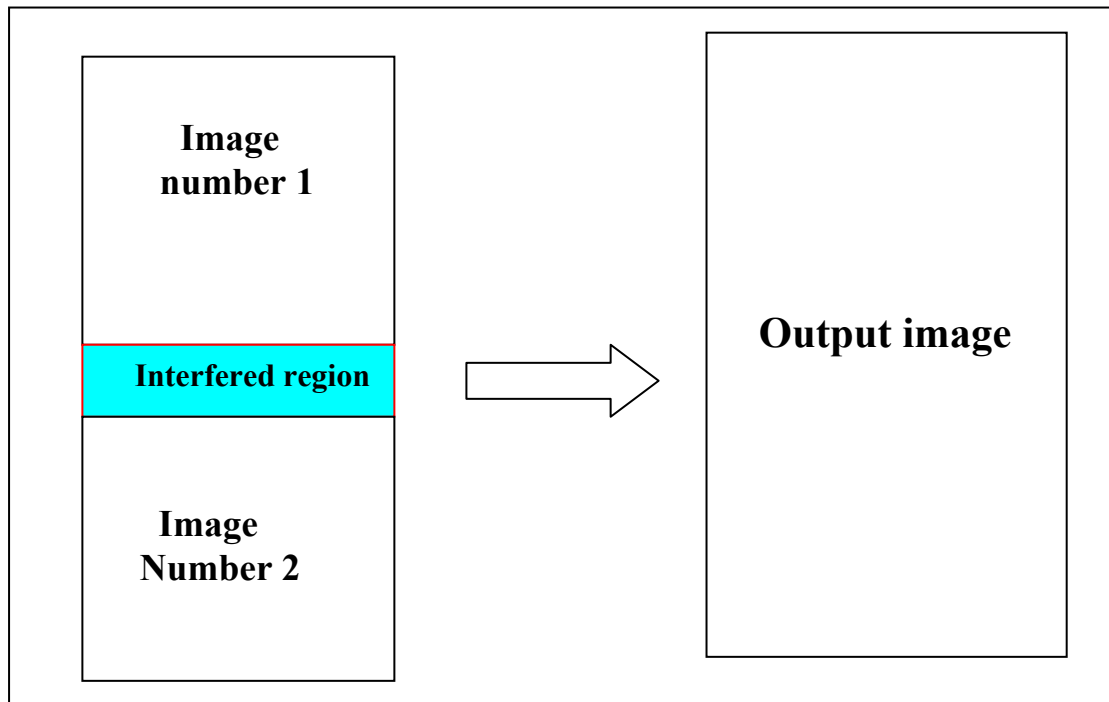


Figure (3-3) illustrate mosaic between two images

3-2-3 Image Enhancement

The goal of image enhancement is to improve the detectable of objects or patterns in a digital image for visual interpretation [1]. Normally, image enhancement involves techniques for increasing the visual distinctions between features in a scene. The objective is to create "new" images from the original image data to increase the amount of information that can be visually interpreted from the data [30].

The most widely used of these techniques is contrast enhancement. Contrast refers to the range of brightness values present on an image. Contrast enhancement is required because digital data usually have brightness ranges that do not match the capabilities of the human visual system. There are two types of contrast enhancement [40].

-linear contrast enhancement (linear stretch):

Linear stretch converts the original digital values into a new distribution, using minimum and maximum values specified. The algorithm then matches the old minimum to the new minimum and the old maximum to the new maximum [40]. So that linear contrast enhancement is done by assigned new DN values to each pixel with the linear relationship [1]:

$$DN_{o(i,j)} = \left\{ \frac{DN_{I(i,j)} - MIN}{MAX-MIN} \right\} * 255 \quad \dots\dots\dots (3-4)$$

Where

$DN_{o(i,j)}$ = output digital number at row i and column j

$DN_{I(i,j)}$ = original digital number of input image at row i and column j

MIN = minimum digital number parameter in input image

MAX= maximum digital number in input image

All pixels with digital number values equal to less than MIN are reassigned the value 0, and pixels with digital number values equal to or greater than MAX are reassigned the value 255.

-Nonlinear contrast enhancement:

One of the most common forms of nonlinear image contrast enhancement is histogram equalization. This method redistributes pixel values, so that there is approximately the same number of pixels with each value within a range [33]. This technique increases contrast in the most populated range of brightness values (the peaks of the histogram) and reduce the contrast in the very light or dark parts of the image (the tails of the histogram). Figure (3-4) illustrates a uniform distribution stretch (histogram equalization) in which the original histogram has been redistributed to produce a uniform population density of pixels.

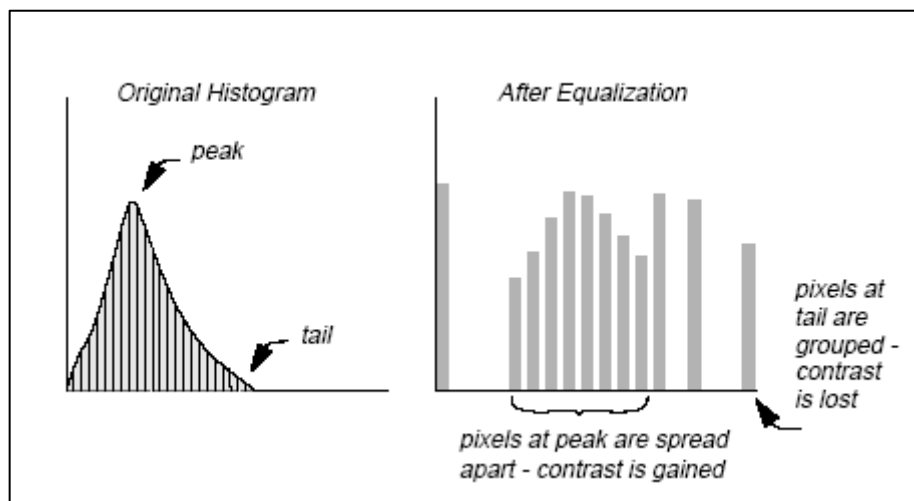


Figure (3-4) histogram equalization [33]

3-2-4 Image Classification:

Image classification attempt to replace visual analysis of the image data with quantitative techniques for automating the identification of features in a scene. Hence; classification process is to categorize all pixels in a digital image into one of several land cover classes or "themes" based on spectral-reflectance characteristics. These categorized data may then be used to produce thematic maps of the land cover present in an image and/or produce summary statistics on the areas covered by each land cover type [30]. Two primary approaches can be used in image classification; Unsupervised classification and Supervised classification.

3-2-4-1 Unsupervised Classification:

Unsupervised classification involves algorithms that examine unknown pixels in an image and aggregate them into number of classes based on the natural groupings or clusters present in the image values [30]. The clustering algorithm is the statistical analysis of the sets of measurement pixels to detect their tendency to form clusters in multidimensional measurement space. Therefore, the clustering algorithm is used in unsupervised classification to partition the sets of data points into a given number of clusters. The points that similar features should be grouped together and points having different features to different groups, for the given data set. This leads to two conditions. First, cluster should exhibit internal cohesion, and points within a cluster should be closed to one another at least within the local area. Secondly, the cluster should have some degree of external isolation. External isolation requires that a relatively empty area of a space exist between dense regions of points [41].

Several methods of unsupervised classification (for example ISODATA), their main purpose being to produce spectral grouping based on certain spectral similarities. In one of the most common approaches, the user has to define the maximum number of clusters in a data set. Based on this, the computer locates arbitrary mean vectors as the centre points of the clusters. Each pixel is then assigned to a cluster by the minimum distance between candidate pixel and each cluster mean. All the pixels have been labeled, recalculation of the cluster centre (cluster mean). The process repeated until the proper cluster centers are found and the pixels are labeled accordingly. The iteration stops when the cluster centers do not change any more (i.e. until reached to a threshold)[41].

The choice of threshold to calculate the minimum distance between two clusters (old cluster and new cluster). A number of methods for finding distance in multidimensional data space are available. One of the simplest is (Euclidean distance) given by this equation, [40]

$$D_{ab} = \left[\sum_{i=1}^N (A_i - B_i)^2 \right]^{(1/2)} \quad \dots\dots\dots(3-5)$$

Where i represent one of N - spectral bands, A , B are pixel value pairs

D_{ab} is the distance between the two pixel value pairs.

So, Euclidean distance has been used as the minimum distance classifier.

The classes that result from unsupervised classification are spectral classes. Because they are based solely on the natural groupings in the image values, the identity of the spectral classes will not be initially known. The analyst must compare the classified data with some form of reference data to determine the identity and informational value of the spectral classes.

3-2-4-2 Supervised Classification

Supervised classification can be defined as process of using samples of known identity to classify pixels of unknown identity. Samples of known identity are those pixels located within training area. The analyst defines training areas by identifying regions on the image that can be clearly matched to areas of known identity on the image [40]. Therefore, the analyst needs to know where to find the classes of interest in the area covered by the image. Supervised classification can be carried out by applying a classification algorithm after the training samples sets have been defined. In the following three classifier algorithms are explained: [42]

1-Parallelepiped Classifier:

Parallelepiped or box classifier based on the range of values in each category training set. This range may be defined by the highest and lowest digital number values or the mean and standard deviation in each band [30].

When the highest and lowest limits are used, they define a box-like area in feature space, which is why called box classifier, as shows in figure (3-5). During classification an unknown pixel if it falls in any of the boxes, it is labeled with class in which box it falls. But pixel that does not fall inside any of the boxes will be assigned the unknown class. The disadvantage of the box classifier is the overlap between the classes. In such a case, a pixel is arbitrary assigned the label of the first box it encounters [42].

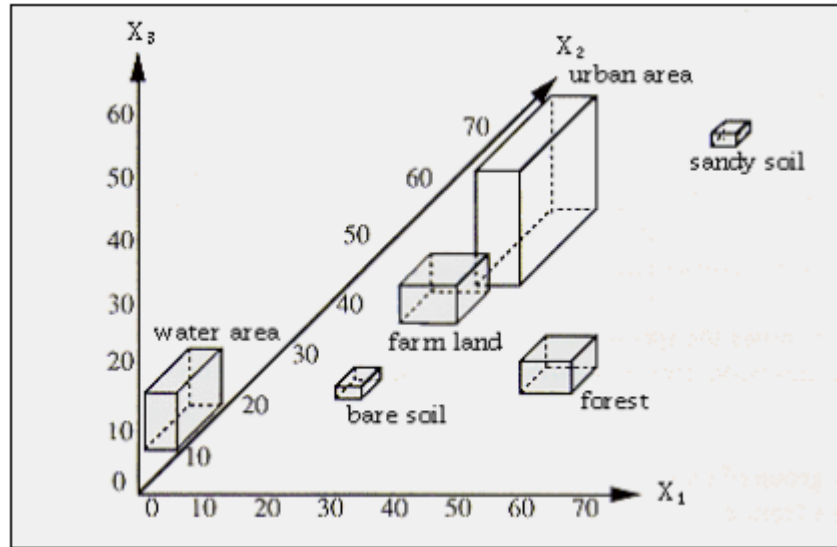


Figure (3-5) Concept parallelepiped classifier in three dimensional feature space[43].

2- Minimum Distance To Mean Classifier:

The basis for the minimum distance to mean classifier is the cluster centers. During classification the Euclidean distances from an unknown pixel to various cluster centers are calculated. The unknown pixel is assigned to that class to which the distance to the mean digital number value of that class is least [43].

The clusters used in this classifier may appear to be the same as those defined earlier for unsupervised classification. However, in unsupervised classification these clusters of pixels were defined according to the "natural" structure of the data. But for supervised classification these clusters are formed by the values of pixels within the training areas defined by the analyst [40]. Figure (3-6) shows the concept minimum distance to mean classifier.

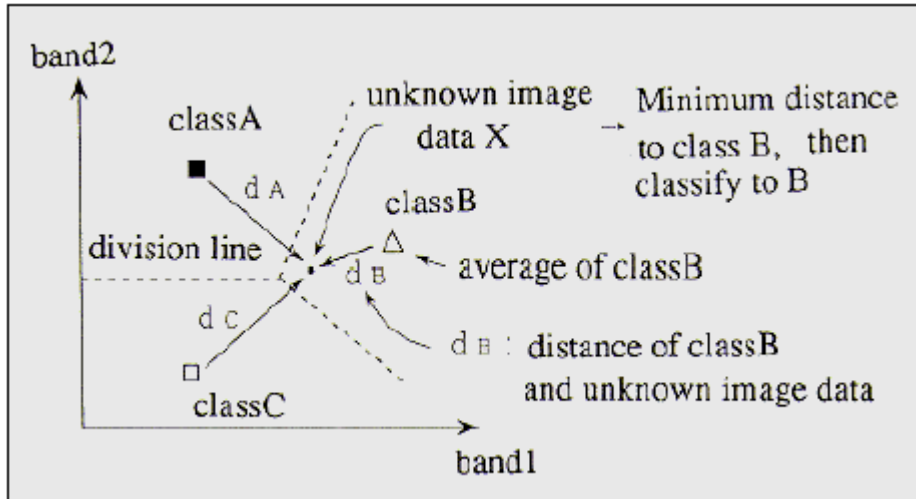


Figure (3-6) concept minimum distance to mean classifier [43]

3- Maximum Likelihood Classifier:

In a parallelepiped classifier and sometimes minimum distance to mean, the overlap of classes is a serious problem because spectral data space cannot then be neatly divided into discrete units for classification. This kind of situation arises frequently because often attention is on classifying those pixels that tend to be spectrally similar rather than those that are distinct enough to be easily and accurately classified by other classifiers. Therefore, used maximum likelihood is considered most common supervised classification methods [40].

The maximum likelihood classifier quantitatively evaluates both the variance and covariance of the category spectral response patterns when classifying an unknown pixel. Under the assumption of normal distribution of the category training data, the distribution of a category response pattern can be completely described by the mean vector and the covariance matrix. Given these parameters, the statistical probability of a given pixel value being a member of a particular land cover category can

be computed and the probability density function for each category can be created. So that the general normal density is given by[30]:

$$P(x) = \frac{1}{(2\pi)^{d/2} |\Sigma|^{1/2}} \text{EXP} \{-1/2 Y^T \Sigma^{-1} Y\} \dots\dots (3-6)$$

Where $Y = x - \mu$

$P(x)$ define the probability of pixel vector of (d) elements pattern defined in term of feature

μ is the d- component mean vector

Σ is the d by d covariance matrix

T is a superscript indicating transposition

Σ^{-1} is the inverse of the covariance matrix

$|\Sigma|$ is the determinant of the covariance matrix

So that the mean vector determines the center of the category, and the shape of the category is determined by the covariance matrix and $(x - \mu)^T \Sigma^{-1} (X - \mu)$ is the contrast.

After evaluating the probability in each category, the pixel would be assigned to the most likely class (highest probability value) or be labeled "unknown", as shows figure (3-7) illustrate maximum likelihood classifier. An extension of the maximum likelihood approach is the Bayesian classifier [30]. The weak point of the Bayesian or maximum likelihood approach to classification is the selection of the training area. So that, if the training are accurate, Bays's approach to classification should be as effective as any that can be applied. If the classes are poorly defined, and the training are not representative often classes to be mapped, the results can be no better than those for other classifiers applied under similar circumstances [40].

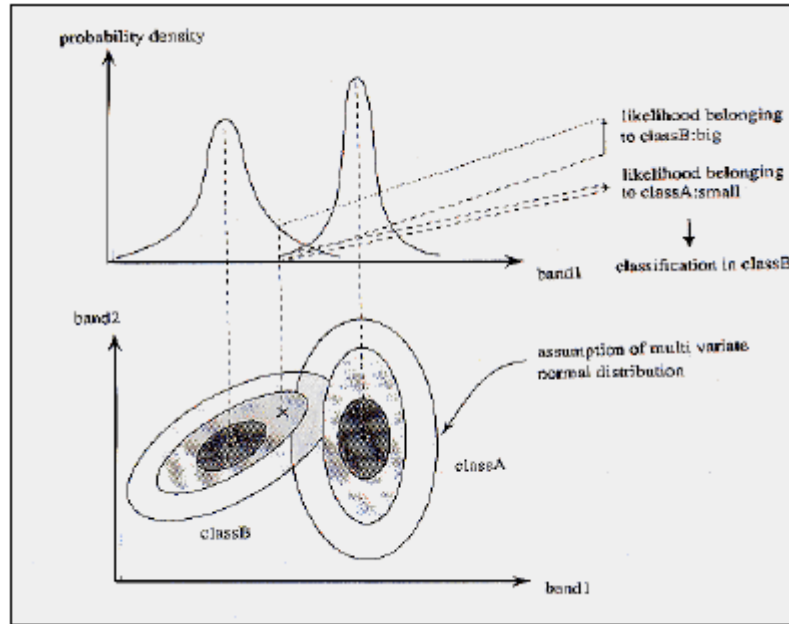


Figure (3-7) concept of Maximum Likelihood classifier [43].

3-3 Vegetation indices:

Vegetation index depend on the spectral reflectance of vegetation, which is very different in near-infrared and red bands. Healthy vegetation should absorb the visible light and reflect most of the near-infrared; on the other hand unhealthy vegetation reflects more visible light and less near-infrared light[19]. The reflection on visible band is related with the pigments in the leaves of plants (chlorophyll), but in the near infrared it depends on the cell structure; (as shows figure (2-6) illustrate spectral reflectance of health vegetation), [28].

There are many vegetation indices models use only the red and near-infrared imagery bands such as, Difference Vegetation Index (DVI), Perpendicular Vegetation Index (PVI), Soil Adjust Vegetation Index (SAVI), Transformed Normalized Difference Vegetation Index (TNVI). The more used and known one is the Normalized Difference Vegetation Index (NDVI) is preferred to the simple index for global vegetation monitoring because NDVI helps compensate for changing illumination

conditions. Normalized Difference Vegetation Index is defined by the following general equation[1]

$$\text{NDVI} = \frac{\text{Near IR band} - \text{red band}}{\text{Near IR band} + \text{red band}} \quad \dots\dots(3-7)$$

The resulting of index value is sensitive to the presence of vegetation on the earth's land surface and can be used to address issues of vegetation, amount and condition. NDVI equation produces values in the range -1 (no vegetation) and +1 (high vegetation). Vegetated areas will generally high values index because of their relatively high near IR reflectance and low visible reflectance; and these areas appeared in image light tones. In contrast water, clouds, and snow have larger visible reflectance than near IR reflected, these features yield negative values. Rock and bare soil areas have similar reflectance in the two bands and result in NDVI near zero. These features in NDVI images appeared black tones. In order to maximize the range values and provide numbers that appropriate to display in 8 bit image, NDVI value must be scaled. This scaling convert atone display. Scaling NDVI value display by the following equation

$$\text{Scaled NDVI} = \left\{ \frac{\text{NDVI} - \text{MIN}}{\text{MAX} - \text{MIN}} \right\} * 255 \quad \dots\dots(3-8)$$

Where NDVI = is the range -1 to +1

Min = minimum value of NDVI

Max = maximum value of NDVI

Using this equation NDVI computed value is scaled to the range of 0 to 255, where computed -1 equals 0 and computed approximately 0 equals 128 and computed 1 equals 255. According this range NDVI values less than 128 represent no vegetation areas and values equals or greater than 128 represent vegetation areas.

Red and near IR data from the following satellite sensors can be for used NDVI:

- Landsat MSS bands 234 (0.6-0.7 μ m) and (0.7-0.8 μ m) or (0.8-1.1 μ m)
- Landsat TM and ETM+ band 3 (0.63-0.69 μ m) and band 4(0.76-0.9 μ m)

3-4 Surface Radiant Temperature:

All remote sensing instruments (air borne, and satellite) are designed to record ground information. Most conventional photography records information in the visible part of electromagnetic spectrum. Thermal instruments operate at longer wavelengths. They are designed for detection of radiant temperature [44]. The radiant temperature emitted from the target (a given information about the targets) on the surface is measured by using thermal infrared band 6 (10.4 – 12.5 μ m) of Landsat 5 TM and Landsat 7 ETM+ images. These information about targets usually scaled and stored as so-called digital numbers that rage from 0 to 255. Therefore for most satellites the digital number to be converted to obtain the surface radiant temperature.

The digital numbers were converted into spectral radiance using the equation [30]

$$L_{\lambda} = \text{Gain} * \text{DN} + \text{Offset} \quad \dots\dots(3-9)$$

Where L_{λ} is the spectral radiance

DN is the digital number of pixel.

Gain is slope of radiance DN conversion function in $\text{W.m}^{-2}.\text{sr}^{-1}.\mu\text{m}^{-1}$

$$\text{Gain} = \text{slope} = \frac{L_{MAX} - L_{MIN}}{255} \quad \dots\dots\dots(3-10)$$

Offset is the rescaled bias which is the intersection of the radiance DN function in $\text{W.m}^{-2}.\text{sr}^{-1}.\mu\text{m}^{-1} = L_{MIN}$, see figure (3-8)

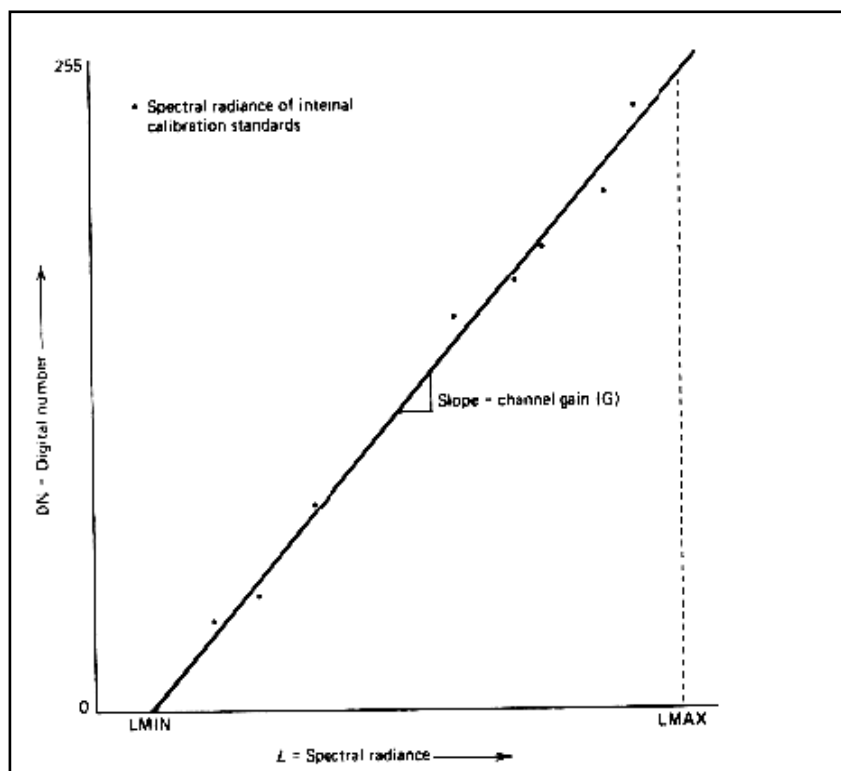


Figure (3-8) linear fit to the calibration data result (relation between radiance and DN values) [30]

Hence equation (1) can be also expressed as [16]

$$L_{\lambda} = \frac{(L_{MAX} - L_{MIN})}{255} * DN + L_{MIN} \quad \dots\dots (3-11)$$

Where L_{MIN} and L_{MAX} are spectral radiances for each band at digital numbers 0 and 255 respectively. For Landsat 5 TM, L_{MIN} and L_{MAX} is

0.124 and 1.560 ($\text{mW}\cdot\text{cm}^{-2}\cdot\text{sr}^{-1}\cdot\mu\text{m}^{-1}$) respectively. For Landsat 7 ETM+ the following references values are given:

Low gain : $L_{\text{MIN}} = 0.0$ $L_{\text{MAX}} = 17.04 \text{ W}\cdot\text{m}^{-2}\cdot\text{sr}^{-1}\cdot\mu\text{m}^{-1}$

High gain : $L_{\text{MIN}}=3.2$ $L_{\text{MAX}} = 12.65 \text{ W}\cdot\text{m}^{-2}\cdot\text{sr}^{-1}\cdot\mu\text{m}^{-1}$

The spectral radiance were converted into surface radiant temperature values by using the relationship[16]:

$$T = \frac{K_2}{\ln[(K_1/L_\lambda) + 1]} \quad \dots\dots\dots(3-12)$$

Where K_1 , K_2 are calibration constants, for Landsat 5 TM constants

$$K_1 = 60.776 \text{ mW}\cdot\text{cm}^{-2}\cdot\text{sr}^{-1}\cdot\mu\text{m}^{-1}$$

$$K_2 = 1260.56 \text{ K}$$

For Landsat 7 ETM+

$$K_1 = 666.09 \text{ W}\cdot\text{m}^{-2}\cdot\text{sr}^{-1}\cdot\mu\text{m}^{-1}$$

$$K_2 = 1282.71 \text{ K}$$

3-5 Correlation between surface radiant temperature and NDVI:

Normalized difference vegetation index (NDVI) has been found to be a good indicator of surface radiant temperature, because the relationship between NDVI and surface radiant temperature was investigated for each land cover type through correlation analysis (pixel by pixel). However, surface radiant temperature values tend to negatively correlate with NDVI values for all land cover types. For example, negative correlation between NDVI and surface temperature implies that higher NDVI and lower surface radiance temperature [16].

CHAPTER FOUR
Practical work (results and discussion)

4-1 Introduction:

This chapter describes and analyzing the methods of remote sensing, the information using digital image processing that including image digital mosaic, geometric correction, image enhancement, image classification, calculating NDVI, surface temperature by using ERDAS IMAGINE 8.4 software.

4-2 Data Used:

Multi-sensor, multi-temporal and multi-spectral image have used to detect changes in Iraqi marshlands, through out interpretation and analyzing these images by using ERDAS IMAGINE8.4. The Landsat images used for this study is shown in table (4-1)

Table (4-1) Illustrate data used in the study

Data type	Acquisition data	Band	Spatial resolution
Landsat MSS	1973	1,2,4	82m
Landsat TM	(7/9/1990)	2,3,4	30m
Landsat TM path166 row38	(7/9/1990)	6	120m
Landsat TM path 166 row39	(7/9/1990)	6	120m
Landsat ETM+	(26/3/2000)	2,3,4	30m
Landsat ETM+ path 166row38	(26/3/2000)	6	60m
Landsat ETM+ path166 row39	(26/3/2000)	6	60m
Landsat ETM+ path166 row38	(6/5/2003)	1,2,3,4	30m
Landsat ETM+ path166 row39	(6/5/2003)	1,2,3,4	30m
Landsat ETM+ path166 row38	(6/5/2003)	6	60m
Landsat ETM+ path166 row39	(6/5/2003)	6	60m
Landsat ETM+ path166 row38	(2/2/2004)	1,2,3,4	30m
Landsat ETM+ path166 row39	(2/2/2004)	1,2,3,4	30m
Landsat ETM+ path166 row38	(2/2/2004)	6	60m
Landsat ETM+ path166 row39	(2/2/2004)	6	60m

4-3 Digital Image Processing:

Many digital image processing techniques are carried out to process the images according to the purpose of application. The image processing which are commonly used for analyzing are given in the following subsections:

4-3-1 Digital Images Mosaic

Image mosaic applied in this study, two images are used together to give a general view of the entire region that is covered by the images, which represent the study area. Image Landsat TM (7/9/1990) band6(thermal band) path 166 row 38 as shown in figure(4-1,A) interfered with image Landsat TM (7/9/1990) band 6 (thermal band)path 166 row 39 as shown in figure (4-1,B) to give image mosaic Landsat ETM+ (7/9/1990) with large area as shown in figure (4-1,C).

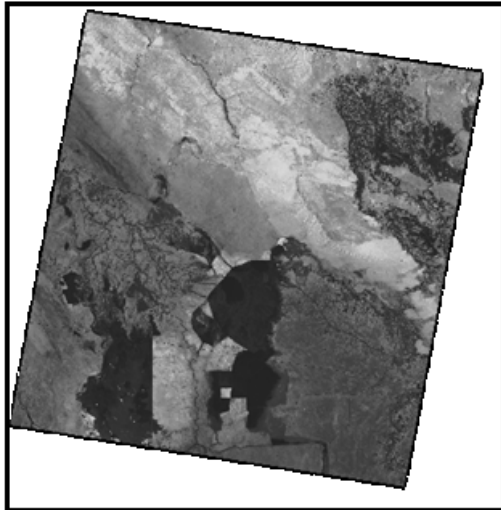
Image Landsat ETM+ (26/3/2000) band6 (thermal band) path166 row38 as shown in figure (4-2, A), interfered with image Landsat ETM+ (26/3/2000) band6 (thermal band) path166 row39 as shown in figure (4-2, B), to give image mosaic as shown in figure (4-2, C).

Image Landsat ETM+ (6/5/2003) band (1,2,3,4) path 166 row38 as shown in figure (4-3,A), interfered with image Landsat ETM+ (6/5/2003) band (1,2,3,4) path166 row39 as shown in figure (4-3,B) to give image mosaic as shown in figure (4-3,C).

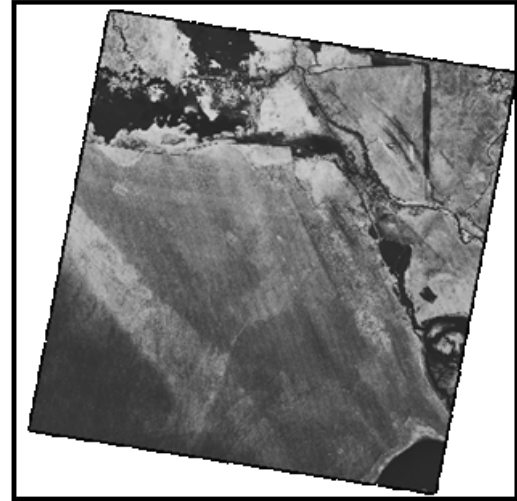
Image Landsat ETM+ (6/5/2003) band6(thermal band) path 166 row38 as shown in figure (4-4,A), interfered with image Landsat ETM+(6/5/2003) band 6(thermal band) path 166 row 39 as shown in figure (4-4,B) to give image mosaic as shown in figure (4-4,C).

Image Landsat ETM+ (2/2/2004) band (1,2,3,4) path 166 row 38 as shown in figure (4-5,A) interfered with image Landsat ETM+ (2/2/2004) band(1,2,3,4) path166 row39, as shown in figure (4-5,B) to give image mosaic as shown in figure (4-5,C).

Image Landsat ETM+ (2/2/2004) band6(thermal band) path166 row38, as shown in figure (4-4,A) interfered with image Landsat ETM+ (2/2/2004)band6(thermal band) path166 row39, as shown in figure (4-6,B) to give image mosaic as shown in figure (4-6,c).



*A- Landsat TM(7/9/1990)
band6 (thermal band)Path 166 Row38*

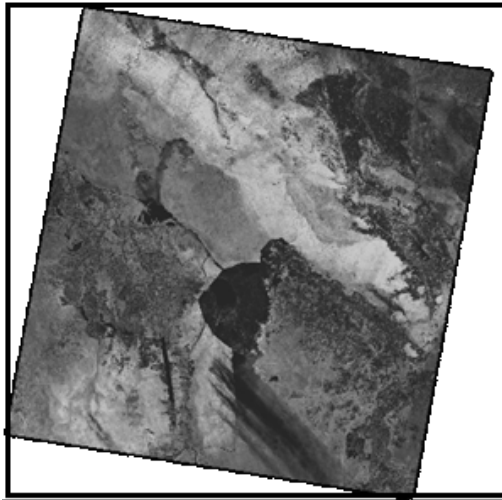


*B- Landsat TM (7/9/1990)
band6(thermal band)Path 166 Row39*

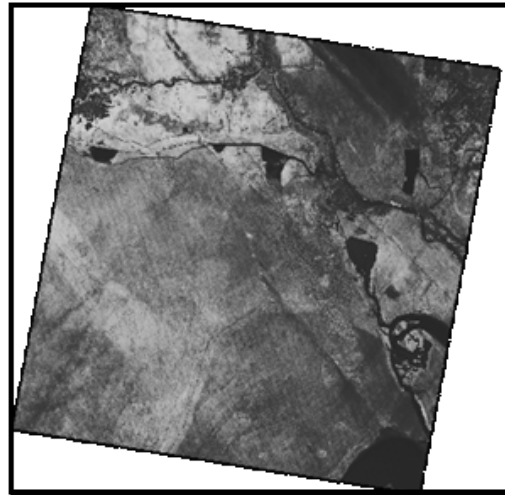


*C- Mosaic Landsat TM (7/9/1990) band6(thermal band) for
Two images (Path166 Row38) and (Path 166 Row39)*

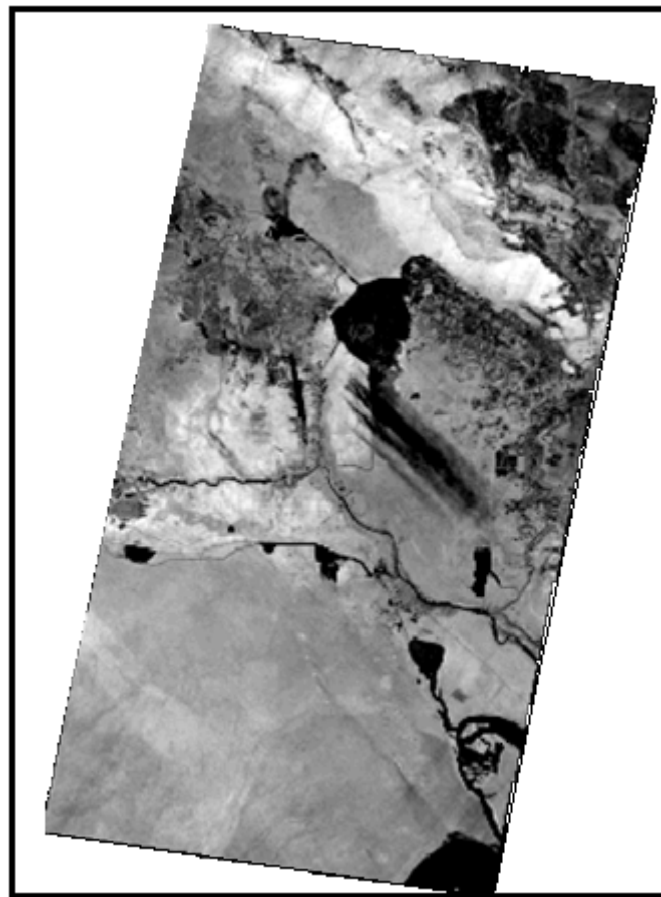
Figure (4-1) show image mosaic for image Landsat ETM+ (7/9/1990) thermal band



A- Landsat ETM+ (26/3/2000) band6 (thermal band) Path 166 Row 38

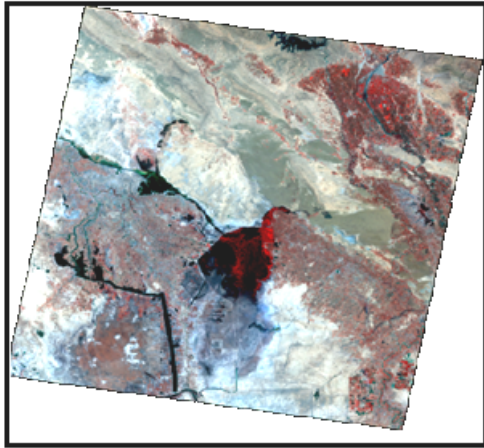


B- Landsat ETM+(26/3/2000) band6 (thermal band) Path 166 Row39

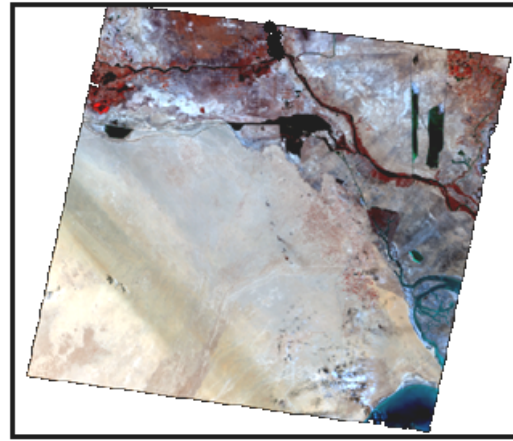


C- Mosaic Landsat ETM+(26/3/2000)band6 (thermal band) for two images (Path 166 Row 38) and (Path 166 Row 39)

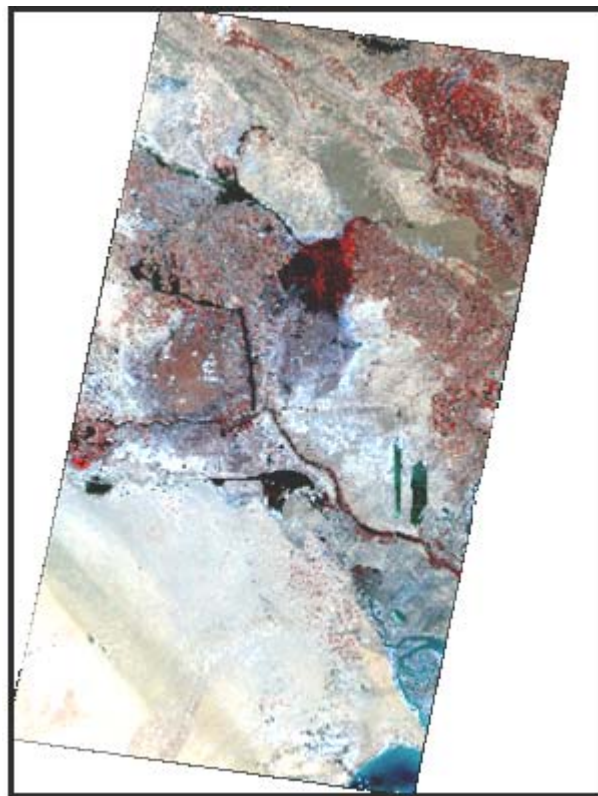
Figure (4-2)show image mosaic for image Landsat ETM+(26/3/2000) thermal band



*A- Landsat ETM+ (6/5/2003)
band(1,2,3,4) Path 166 Row 38*

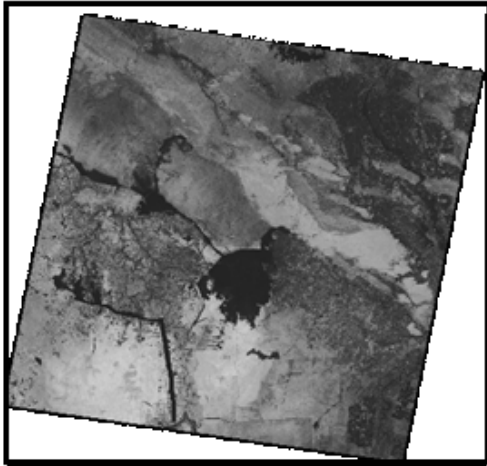


*B- Landsat ETM+(6/5/2003)
band(1,2,3,4) Path 166 Row 39*

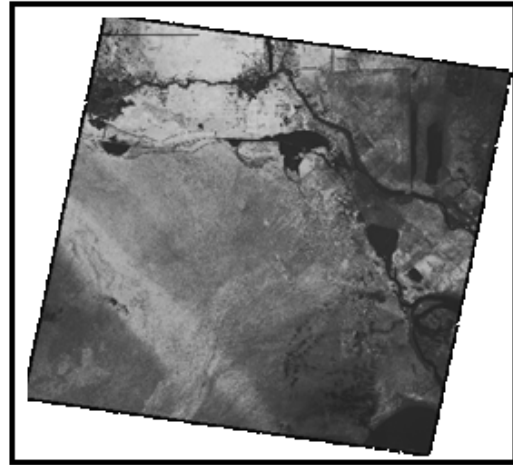


*C-Mosaic Landsat ETM+ (6/5/2003)band(1,2,3,4) for
two images (Path166 Row38) and (Path 166 Row39)*

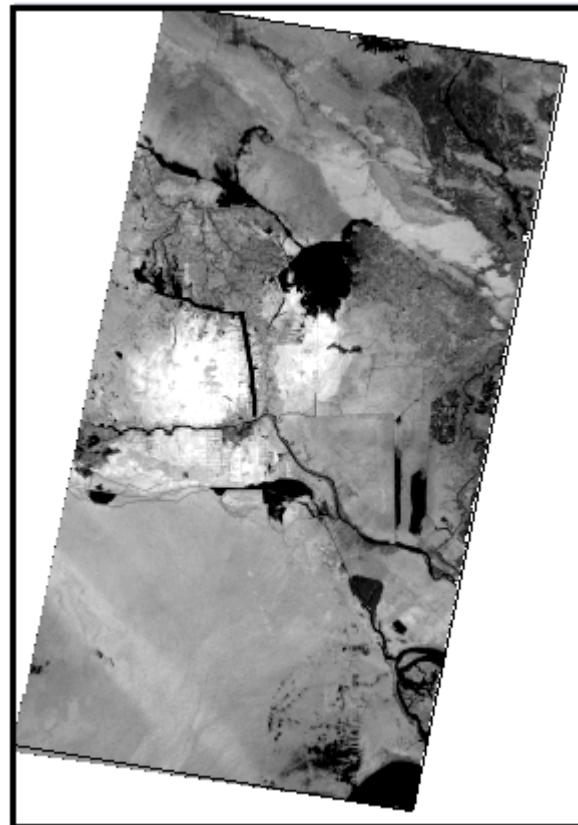
Figure (4-3) show image mosaic for image Landsat ETM+(6/5/2003)band(1,2,3,4)



A- Landsat ETM+ (6/5/2003) band6 (thermal band)Path166 Row 38

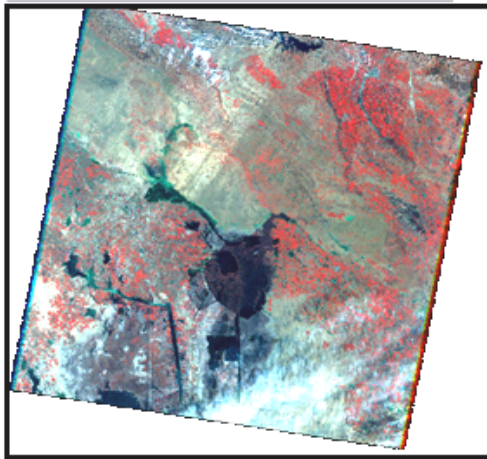


B- Landsat ETM+(6/5/2003) band6 (thermal band) Path 166 Row 39

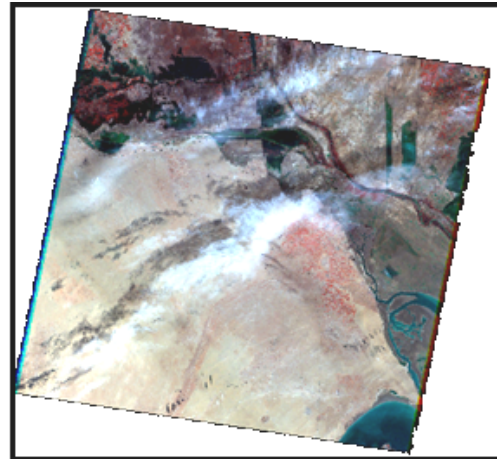


C- Mosaic Landsat ETM+(6/5/2003) band6(thermal band) for two images (Path 166 Row 38) and (Path 166 Row 39)

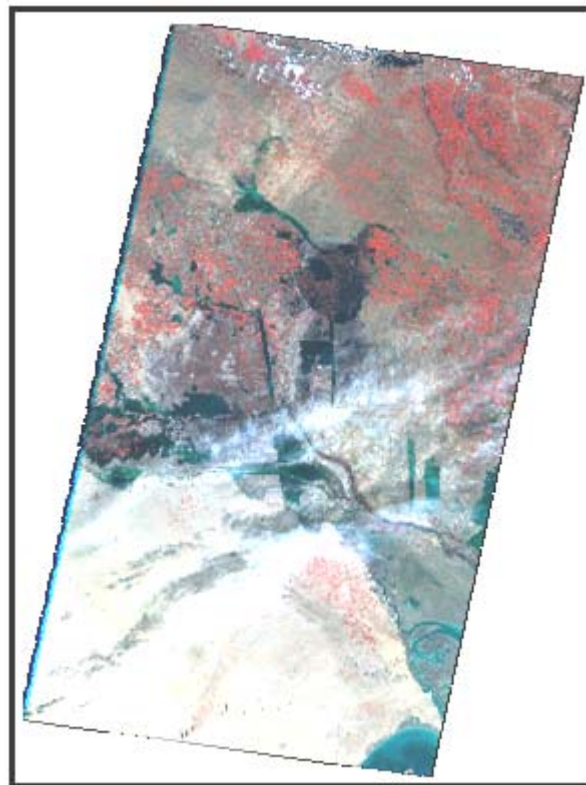
Figure (4-4)show image mosaic for image Landsat ETM+(6/5/2003) thermal band



*A- Landsat ETM+ (2/2/2004)
band(1,2,3,4) Path 166 Row 38*

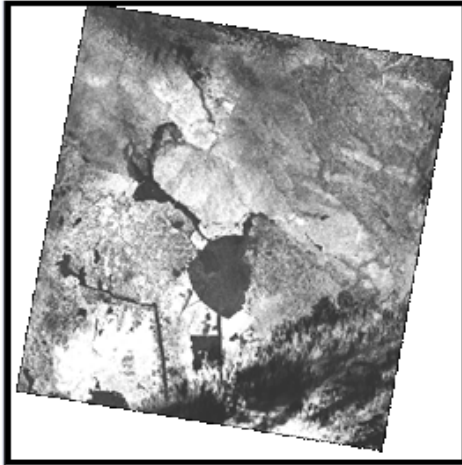


*B- Landsat ETM+ (2/2/2004)
band(1,2,3,4) Path 166 Row 39*

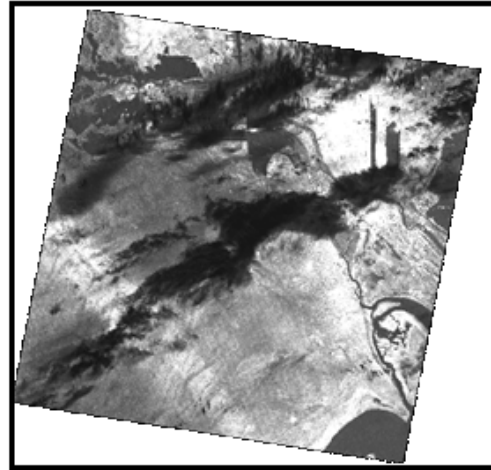


*C- Mosaic Landsat ETM+ (2/2/2004)band(1,2,3,4) for
two images (Path 166 Row 38) and (Path 166 Row 39)*

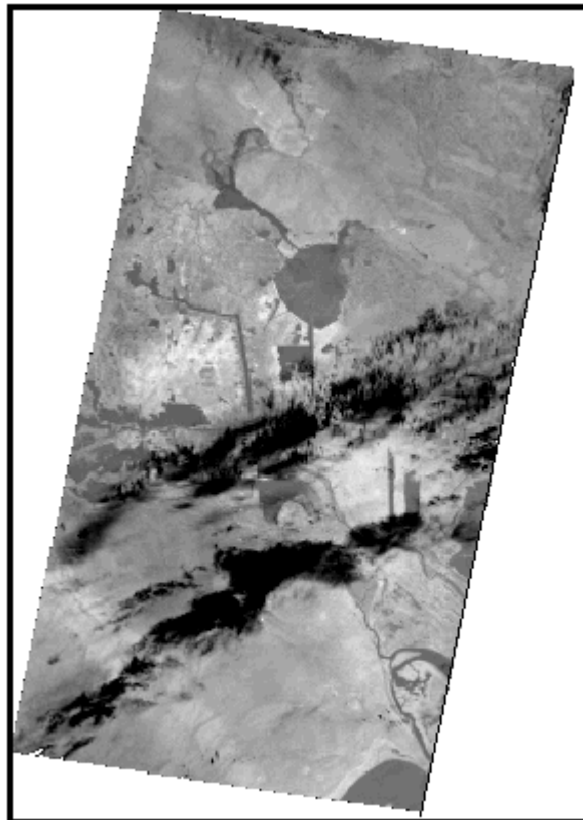
Figure(4-5)show image mosaic for image Landsat ETM+ (2/2/2004)band(1,2,3,4)



A- Landsat ETM+ (2/2/2004)band6 (thermal band)Path166Row38



B- Landsat ETM+(2/2/2004)band6 (thermal band) Path 166 Row39



C- Mosaic Landsat ETM+ (2/2/2004) band6 (thermal band) for two images (Path 166 Row 38)and (Path 166 Row 39)

Figure (4-6)show image mosaic for image Landsat ETM+ (2/2/2004)(thermal band)

4-3-2 Geometric Correction:

The term registration or rectification used to describe geometric correction. Registration is an important stage in the change detection, so that repeated Landsat images of the same area must be registered because of differences in spacecraft position, altitude, and attitude [45].

In this study registration process is conducted. Landsat ETM+ dated (2004) image is used as reference image to geometric correction of Landsat MSS dated (1973), Landsat TM (1990) and Landsat ETM+ (2000).

For Landsat MSS 1973 image correction, 15 GCPs are selected and well distributed on image, RMS error is 0.045 pixel. In case of correction Landsat TM (7/9/1990) image, 25 GCPs distributed on all image are used, RMS error is 0.64 pixel. In case of correction of Landsat ETM+(26/3/2000) image, 25 GCPs distributed on the image are used, RMS error is 0.069 pixel.

The linear transformation (1st- order polynomial) was applied to transform coordinates of reference image to input image. A nearest-neighbors resampling method used to determine the new digital numbers value for each of the pixel in the new transformed image.

Table (4-2) illustrates the position of the GCPs on the input image Landsat ETM+ (2/2/2004). Figure (4-7) shows locations of 15 GCPs are distribution on input image 1973 (un-corrected) and reference image (2/2/2004) (corrected).

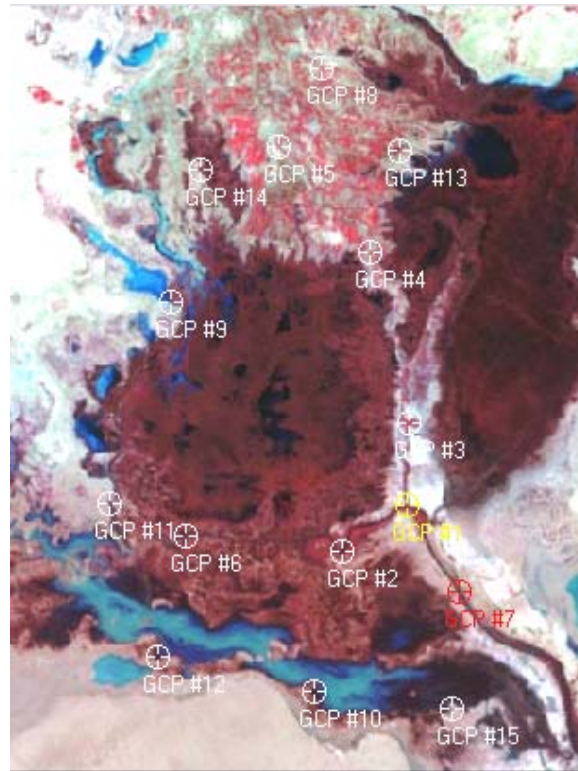
Table (4-2) the position of the GCPs on the input image 1973 and the reference image (2/2/2004)

No. GCPs	X Input	Y Input	X Reference	Y Reference	X Residual	Y Residual	RMS error
1	360.105	-297.012	733837.378	3432718.581	0.015	0.063	0.064
2	320.316	-324.033	720179.635	3424079.647	0.023	-0.025	0.036
3	360.699	-249.205	733905.501	3448142.130	-0.023	0.050	0.055
4	337.538	-150.326	725665.352	3480106.666	0.000	0.013	0.013
5	283.496	-89.752	706862.181	3499796.822	0.007	-0.016	0.017
6	227.439	-314.544	688086.649	3427405.930	-0.030	-0.004	0.031
7	390.127	-347.082	744318.877	3416449.284	-0.009	-0.020	0.022
8	308.119	-43.620	715251.976	3514606.631	0.043	-0.048	0.064
9	218.475	-179.082	684645.707	3471142.108	-0.022	-0.028	0.036
10	304.467	-404.188	714889.772	3398248.479	-0.059	-0.043	0.073
11	181.621	-295.619	672241.000	3433646.000	0.011	0.013	0.017
12	210.839	-384.599	682563.032	3404858.709	0.039	0.048	0.061
13	355.069	-91.559	731551.173	3499031.844	-0.033	0.036	0.049
14	236.087	-102.365	690531.528	3495862.556	-0.002	0.001	0.002
15	386.161	-414.432	743141.712	3394716.986	0.040	-0.040	0.057

Total RMS error = 0.045 pixel

UTM projection

WGS 84 Spheroid and Datum



A- Image Landsat MSS 1973 band (1,2,4) (un-corrected)



B- Image Landsat ETM+ (2/2/2004) band(1,2,3,4) (corrected)

Figure (4-7) Show locations of the GCPs on the two images

After mosaic image production and geometric correction, study area represent Iraqi marshlands including (central marshes, Al- Hammar marsh, part of Al-Hawizah marsh) have selected. Figure (4-8) illustrate the mosaic Landsat TM (7/9/1990) band6 and location of the study area.

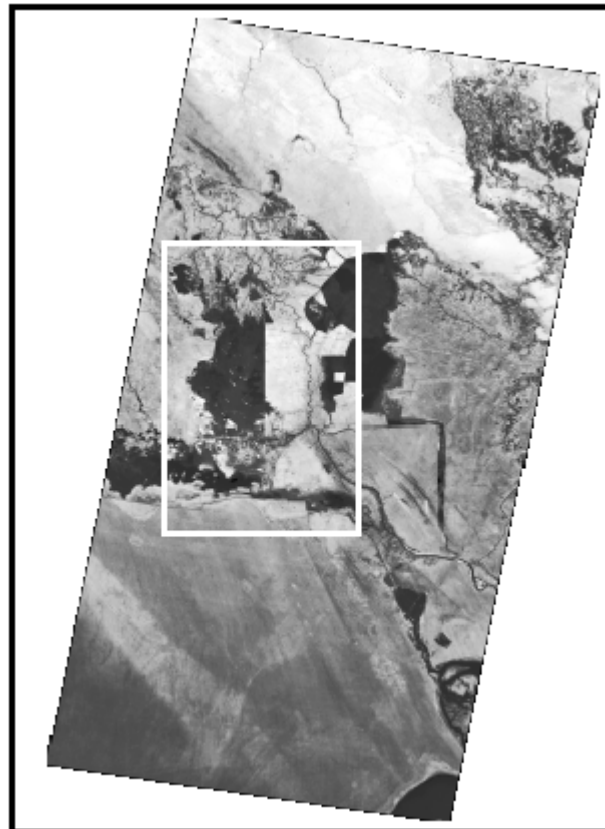


*Figure (4-8) Illustrate image inside the polygon represent study area
(7/9/1990) band6*

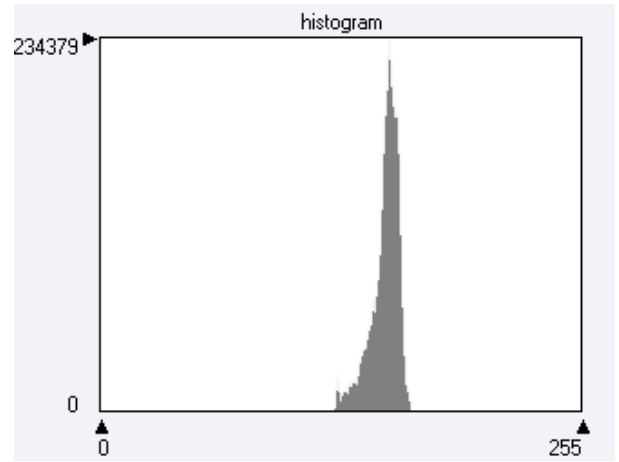
4-3-3 Image Enhancement:

The principle objective of enhancement techniques is to process the image so that the result is more suitable than the origin. A digital image enhancement used to increase the contrast among the various feature. Such that for low contrast, the histogram is concentrated within a small region of the gray scale. The principle of the contrast enhancement is to redistribute the gray values of the original image to the full range of the gray scale from 0 to 255.

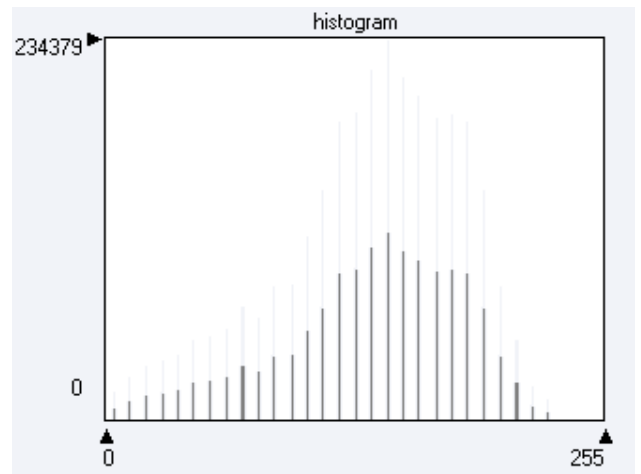
Contrast stretching enhancement is used to increase level contrast for thermal band of Landsat ETM+ (26/3/2000) image. Figure (4-9) shows Landsat ETM+ (26/3/2000) band6 image for study area and its histogram before and after applying contrast stretching.

Figure (4-10) shows Landsat ETM+ (6/5/2003) band 6 for study area and its histogram before and after applying contrast stretching. Image contrast for Landsat ETM+ (6/5/2003) image was not applied for technical reason.

Histogram equalization (non-linear contrast) used for Landsat ETM+ image (2/2/2004) band 6 which represent study area. Figure (4-11) shows Landsat ETM+ (2/2/2004) band 6 image for study area and its histogram before and after applying histogram equalization technique. It is clearly seen that histogram equalization reduce contrast in very light or dark area and to extend the middle gray levels to word low and high ends of the gray levels.

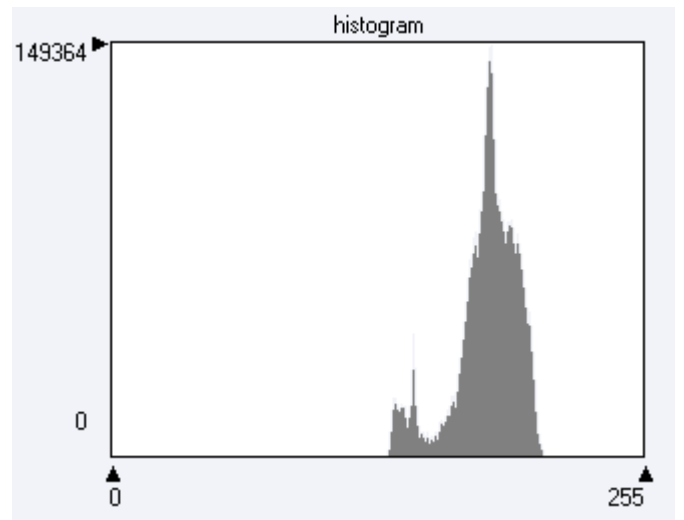


A- Before applying contrast stretching

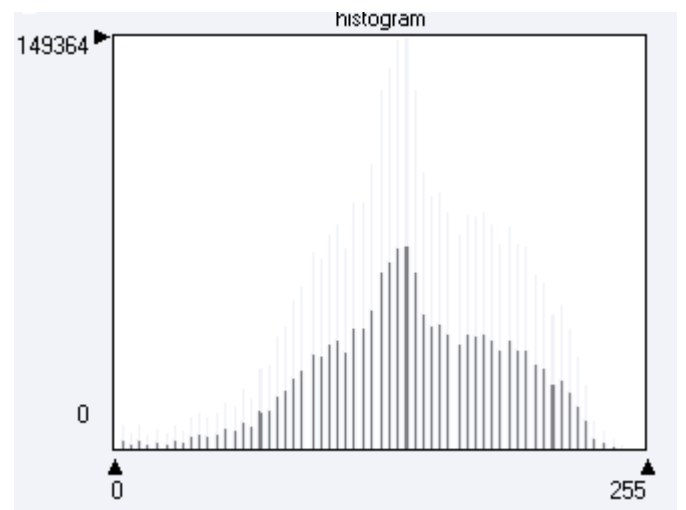


B-After applying contrast stretching

Figure (4-9) show Landsat ETM+ (26/3/2000) band6 image for study area and its histogram before and after applying contrast stretching.

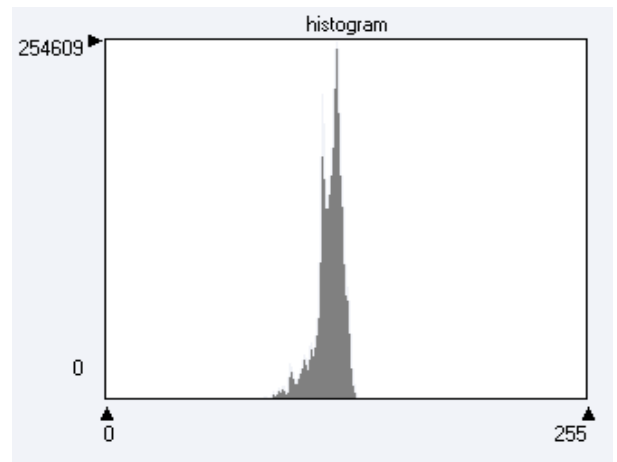


A- Before applying contrast stretching

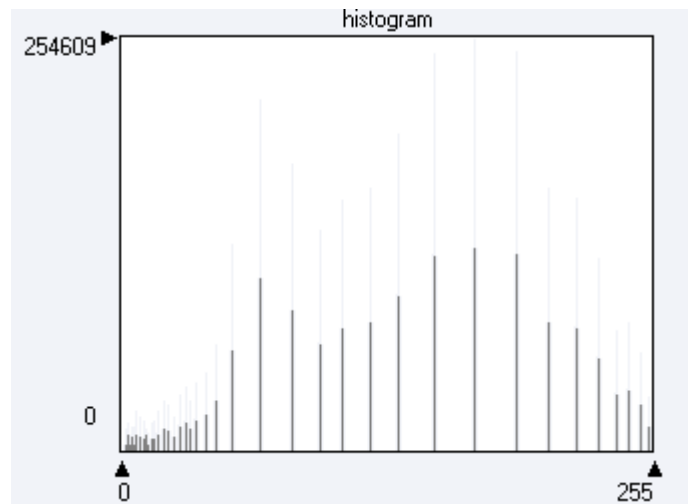


B- After applying contrast stretching

Figure (4-10) show Landsat ETM+ (6/5/2003)band 6 for study area and its histogram before and after applying contrast stretching.



A - Before applying the histogram equalization



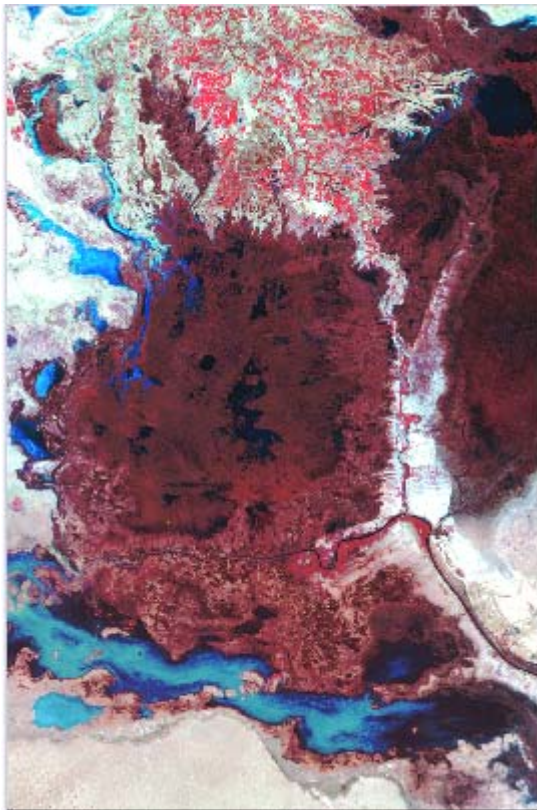
B- After applying histogram equalization

Figure (4-11) show Landsat ETM+ (2/2/2004) band 6 image for study area and its histogram before and after applying histogram equalization technique.

4-3-4 Image Classification:

Classification is the process of grouping pixels or regions of the image into classes representing different ground-cover types [44]. Two main digital analysis techniques are available for the classification of remotely sensed, unsupervised and supervised classification.

Both unsupervised and supervised classification techniques are used for Landsat images classification. The study area images were classified to five classes for each technique of classification. Figure (4-12) shows Landsat images for study area which are used in classification technique.



*A-Landsat MSS image 1973,
band(1,2,4) for study area*



*B- Landsat TM image (7/9/1990)
band (2,3,4) for study area*



C- Landsat ETM + image(26/3/2000) band(2,3,4) for study area



D- Landsat ETM+ image (6/5/2003) band (1,2,3,4) for study area



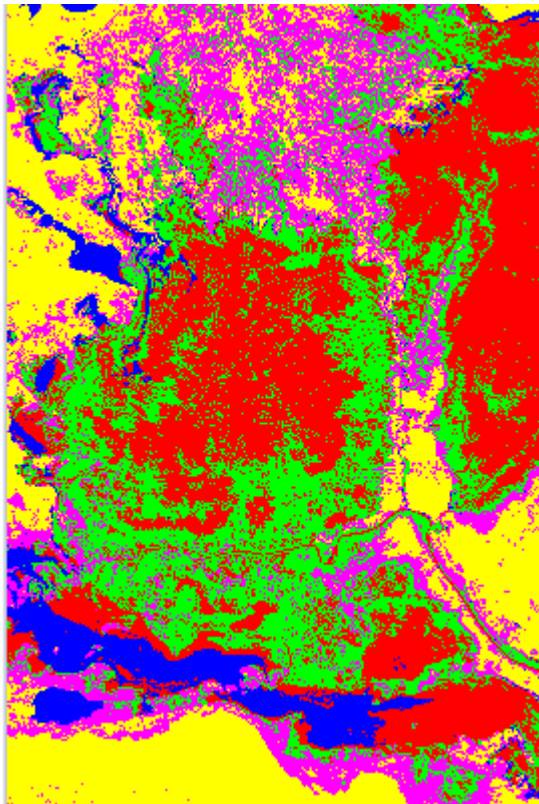
E- Landsat ETM+ image (2/2/2004) band (1,2,3,4) for study area

Figure (4-12) Landsat images for study area before applying classification technique

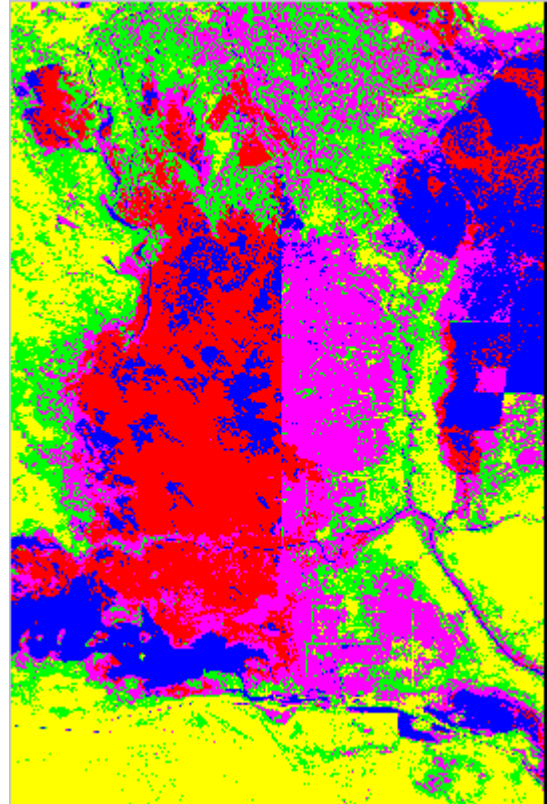
4-3-4-1 Unsupervised Classification:

Unsupervised classification is a process that separates the pixels of the image based upon their reflectance values into classes or clusters with no direction from the analyst. Therefore used this technique to give an idea about spectral pattern of the study area before applying supervised classification that needed the knowledge of the geography of the region and experience with the spectral properties to select training area. In this technique Landsat images that represent the study area at different time, are classified by using Isodata method.

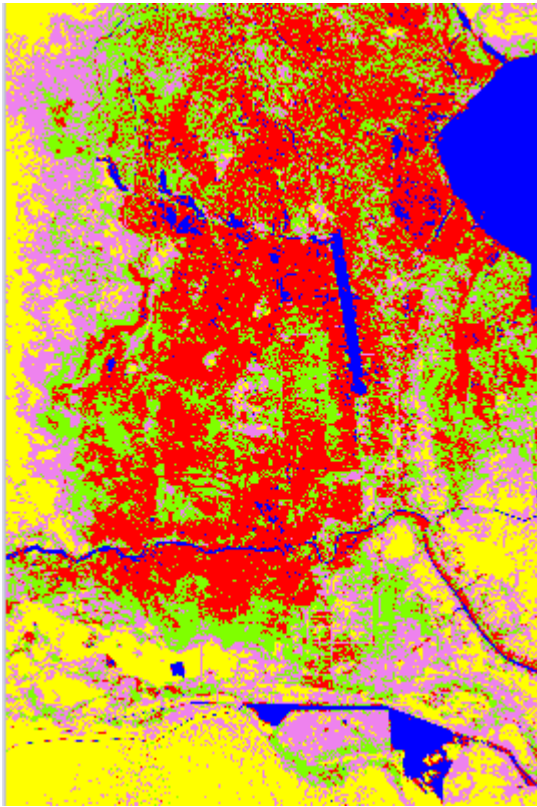
In this method Landsat images are classified into five classes (water, wet land, barren land, marsh vegetation, agriculture). Table (4-3) and figure (4-13) shows results of unsupervised classification by using Isodata method.



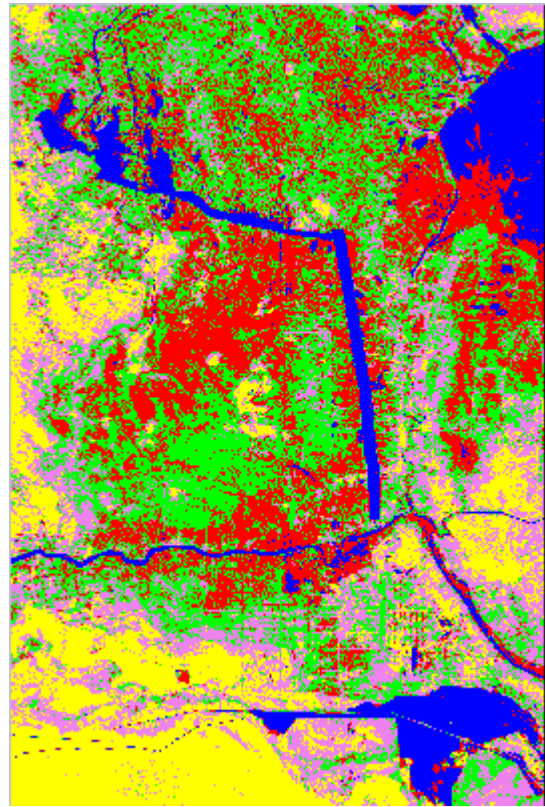
A-Unsupervised classification of Image Landsat MSS1973 by Using Isodata method



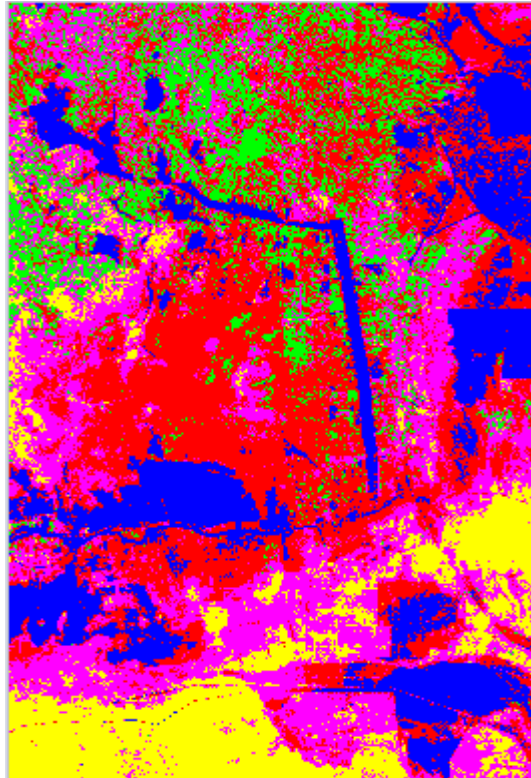
B-Unsupervised classification of image Landsat TM 1990 by using Isodata method



D-Unsupervised classification of Image Landsat ETM+ 2000 by Using ISodata method





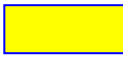


E-Unsupervised classification of image Landsat ETM+ 2003 by using Isodata method



E- Unsupervised classification of Image Landsat ETM+2004 by using Isodata method

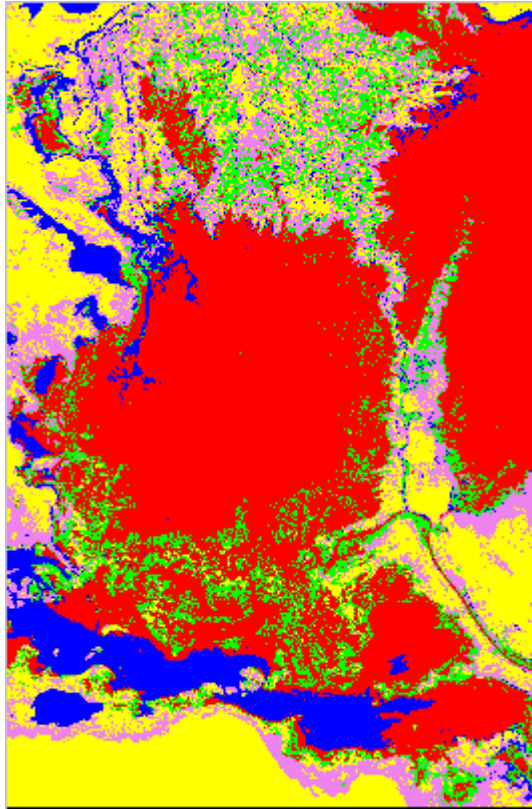
Figure (4-13) illustrate unsupervised classification of Landsat images at different times

Table (4-3) results of unsupervised classification for Landsat images by using ISOdata method

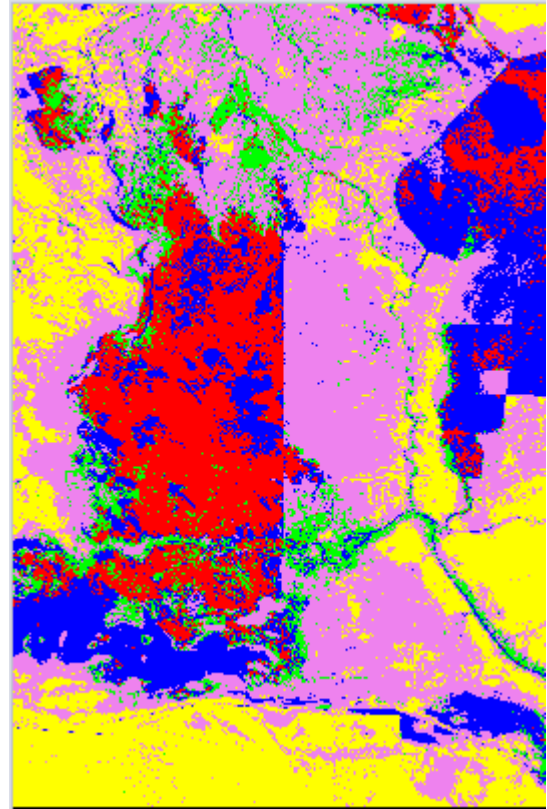
Class name	Color Name	Landsat MSS 1973	Landsat TM (7/9/1990)	Landsat ETM+ (26/3/2000)	Landsat ETM+ (6/5/2003)	Landsat ETM+ (2/2/2004)
		No. pixels	No. pixels	No. pixels	No. pixels	No. pixels
Water		603219 6.4%	2213165 15%	686457 6.9%	1382986 9.7%	2294051 17.9%
Wet land		1720275 18.3%	3452011 23.5%	2017000 20.2%	2976518 21%	3252974 25.4%
Barren land		1952381 20.7%	3278878 22.3%	1777995 17.8%	2466326 17.4%	1632677 12.7%
Marsh vegetation		2788790 29.6%	2653526 15%	3033643 30.4%	3273195 23.1%	4177475 32.6%
Agriculture land		2349025 24.9%	3111693 21.2%	2459075 24.6%	4099621 28.9%	1457110 11.4%

4-3-4-2 Supervised Classification:

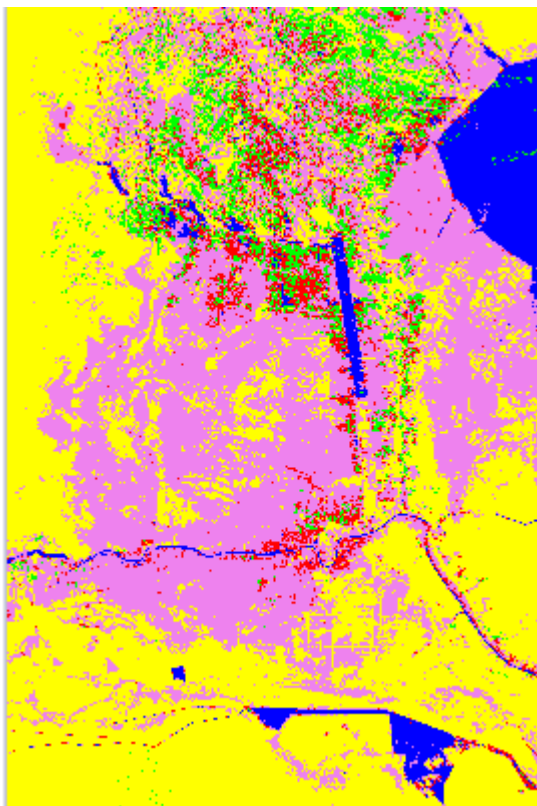
Supervised classification performed after selecting training area, supervised classification with Maximum Likelihood algorithm was produced to classify the Landsat images that represent study area at different times, as shown in figure (4-14). The Landsat images were classified to five classes represent water, wet land, barren land, marsh vegetation, agriculture. Table (4-4) shows the results of supervised classification by using Maximum Likelihood methods.



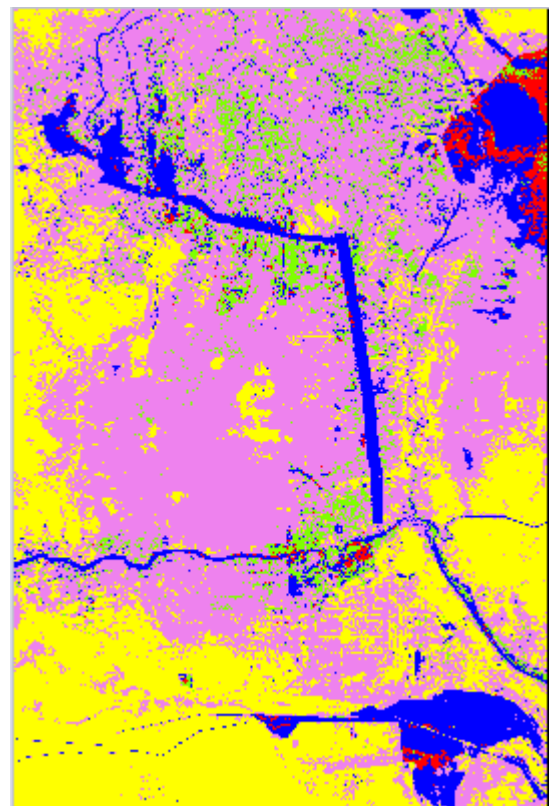
A- Supervised classification of Image Landsat MSS 1973 by using maximum likelihood method



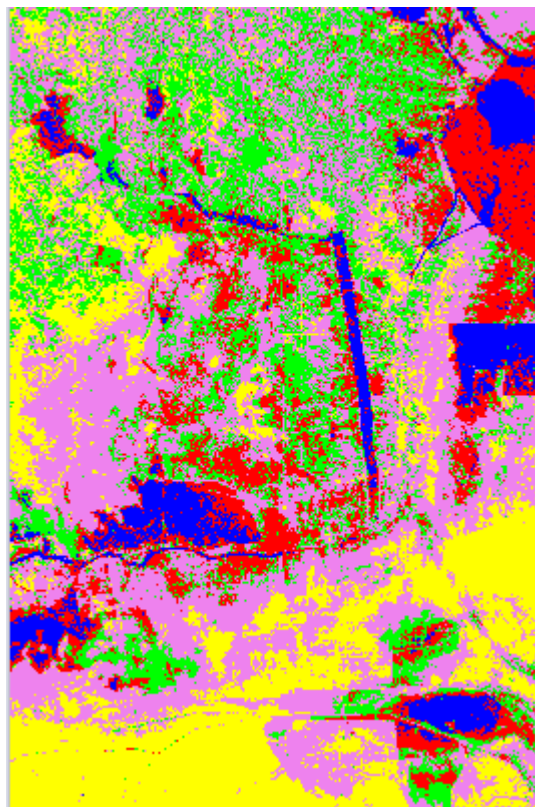
B- Supervised classification of image Landsat TM 1990 by using maximum likelihood method



C- Supervised classification of image Landsat ETM+ 2000 by using maximum likelihood method



D- Supervised classification of image Landsat ETM+ 2003 by using maximum likelihood method



*E- Supervised classification of image Landsat ETM+ 2004
by using maximum likelihood method*

*Figure (4-14) illustrate supervised classification of Landsat images at different
Times by using maximum likelihood Method*

Table (4-4) show results supervised classification for Landsat images by
using maximum likelihood method






Class Name	Color Name	Landsat	Landsat	Landsat	Landsat	Landsat
		MSS 973	TM (7/9/1990)	ETM+ (26/3/2000)	ETM+ (6/5/2003)	ETM+ (2/2/2004)
		No. Pixels	No. pixels	No. pixels	No. pixels	No. pixels
Water		814737 8.7%	2493157 16.9%	564469 5.7%	1424095 10%	856476 6.7%
Wet land		1370967 14.6%	5657289 38.5%	3746737 37.6%	7250615 51.1%	4911379 38.3%
Barren land		1963580 20.9%	3257187 22.1%	4675944 46.9%	4366522 30.8%	2674964 20.9%
Marsh vege.		4207292 44.7%	2140654 14.6%	463932 4.7%	215395 1.5%	1840023 14.6%
Agri. land		1057114 11.2%	1160986 8%	523088 5.2%	942019 6.6%	2531445 19.8%

Figure (4-15) illustrates the comparative analysis of Landsat (1973-2004) imagery based on supervised classification by using maximum likelihood method.

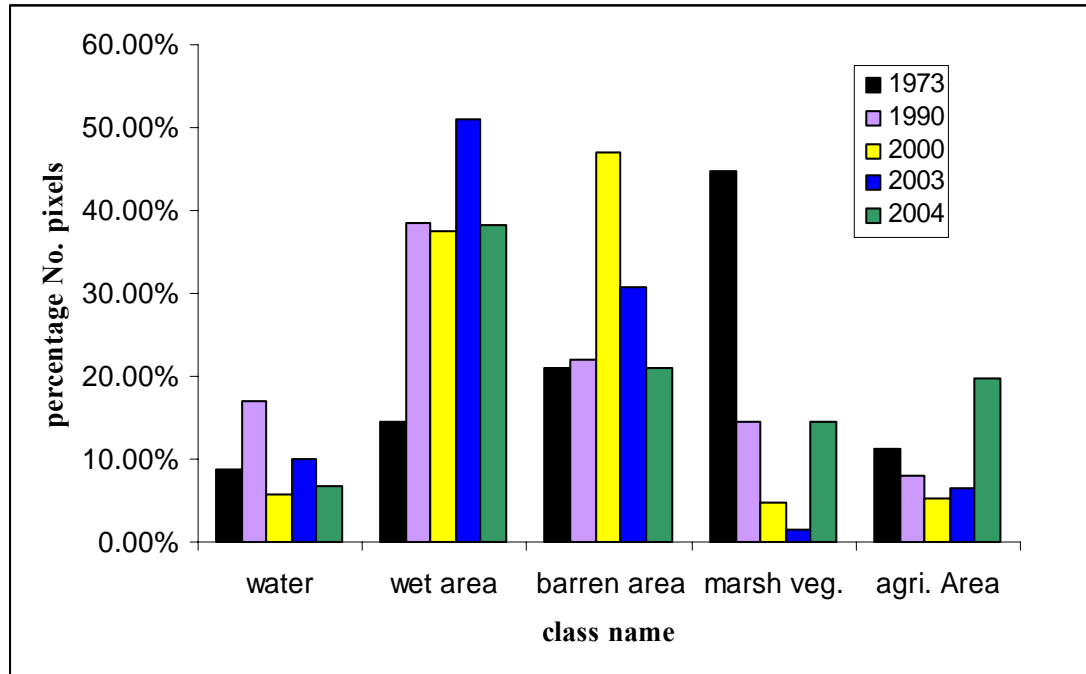


Figure (4-15) Show area percentage for each class for 1973, 1990, 2000, 2003, 2004

It is clear that from figure (4-15) and table (4-4) in 1973 marsh vegetation area (percentage number of pixels) is high, such that dense vegetation marsh covered the area of water. The areas of vegetation marsh and water started decreasing since 1990 and reach the lowest value in 2000 because of the desiccation marshes. This desiccation causing increase the wet area and barren area, so that in 2000 barren area increase 24.8% than in 1990. The resultant of the supervised classification appearance that reflooding marshes such that water increase about 4.3% than in 2000, but this increases not effected into vegetation marsh and causing increasing in wet area. In 2004 the present fog in Landsat ETM+ 2004 effected into the result of the supervised classification, so that it appeared increase in vegetation marsh but decrease water.

4-4 Normalized Difference Vegetation Index (NDVI):

Normalized difference vegetation index used because has been found to be good indicator for vegetation and land use/ land cover changes. It has been found that NDVI good indicator of surface temperature. NDVI computed from the equation (3-7) as

$$\text{NDVI} = \frac{\text{Near IR band} - \text{Red band}}{\text{Near IR band} + \text{Red band}}$$

The original NDVI has the values between -1 and +1, but in this study it was transformed into images 8 bit (0 – 255) according equation (3-8) is

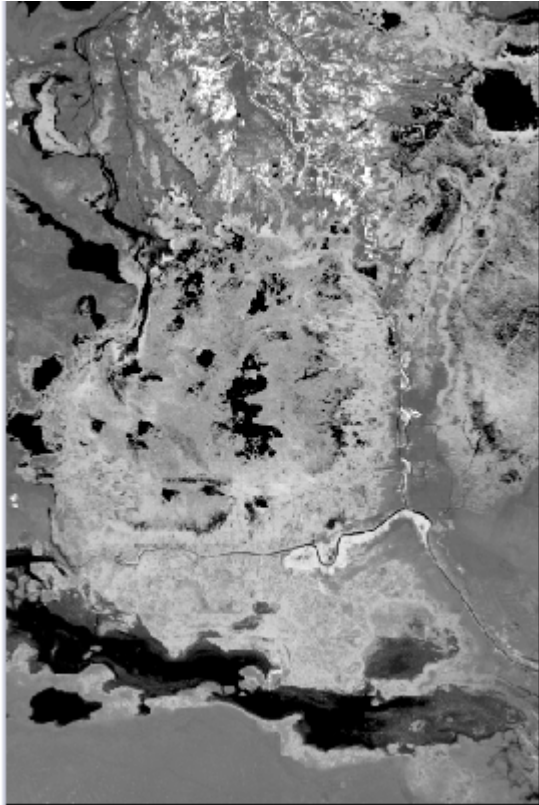
$$\text{Scaled NDVI} = \left\{ \frac{\text{NDVI} - \text{MIN}}{\text{MAX} - \text{MIN}} \right\} * 255$$

Where NDVI = is the range -1 to +1

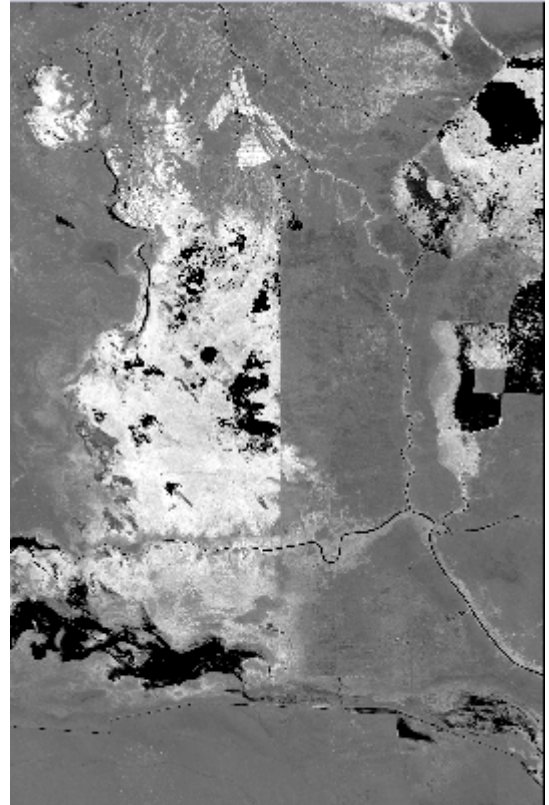
Min = Minimum value of NDVI

Max = Maximum value of NDVI

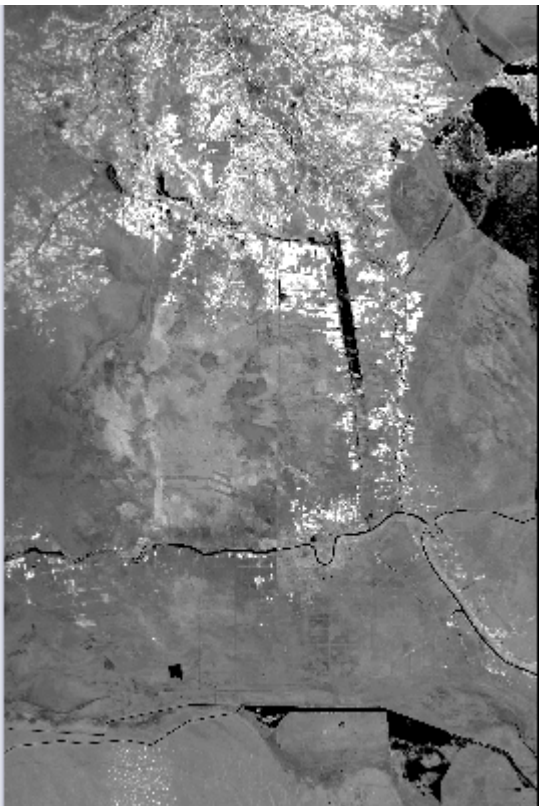
The NDVI image computed from Landsat MSS 1973, Landsat TM (7/9/1990), Landsat ETM+ (26/3/2000), Landsat ETM+ (6/5/2003), and Landsat ETM+ (2/2/2004) images. Figure (4-16) shows NDVI images for study area. These images display dark area (low value NDVI) which represents no vegetation such as water, wet land and barren land; while bright area (high value NDVI) represent high vegetation such as agriculture land and vegetation marsh land .



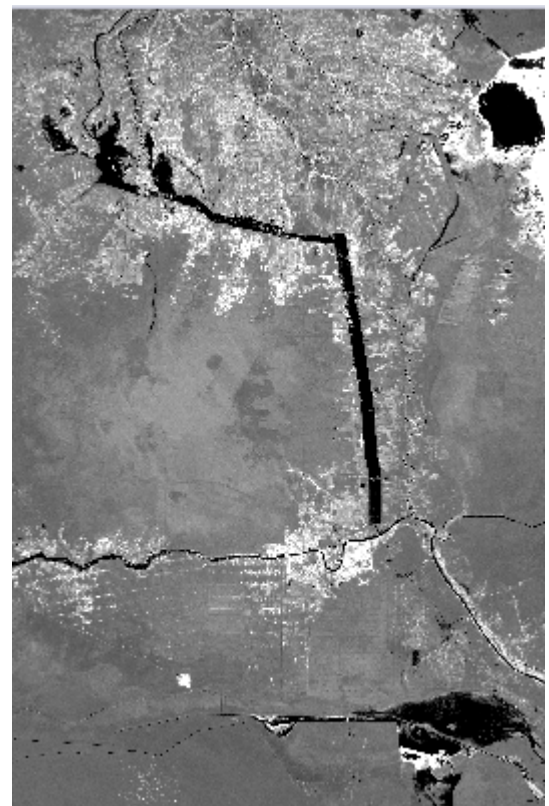
A- NDVI for image Landsat MSS 1973



*B- NDVI for image Landsat TM
(7/9/1990)*



*C- NDVI for image Landsat ETM+
(26/3/2000)*



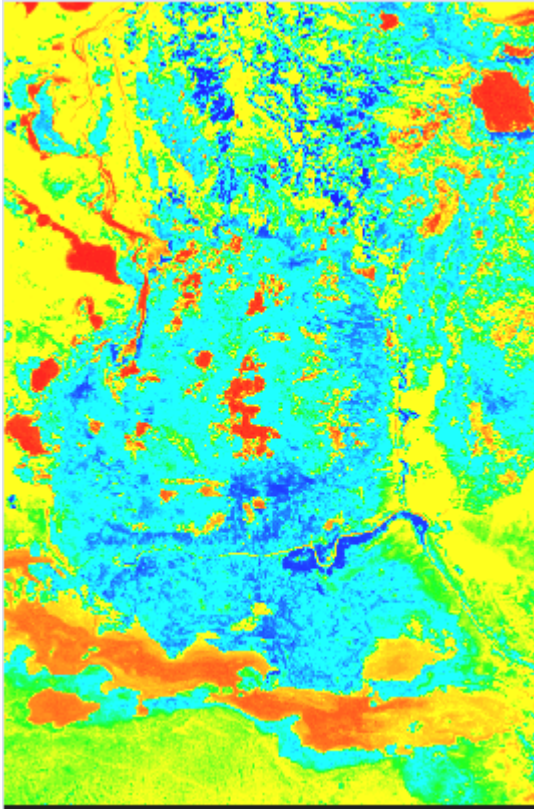
*D- NDVI for image Landsat ETM+
(6/5/2003)*



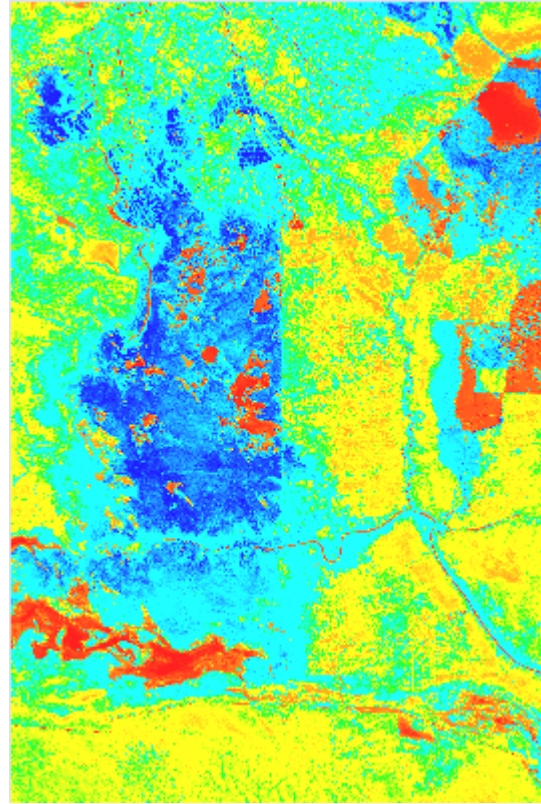
E- NDVI for image Landsat ETM+ (2/2/2004)

Figure (4-16) show NDVI images for image Landsat

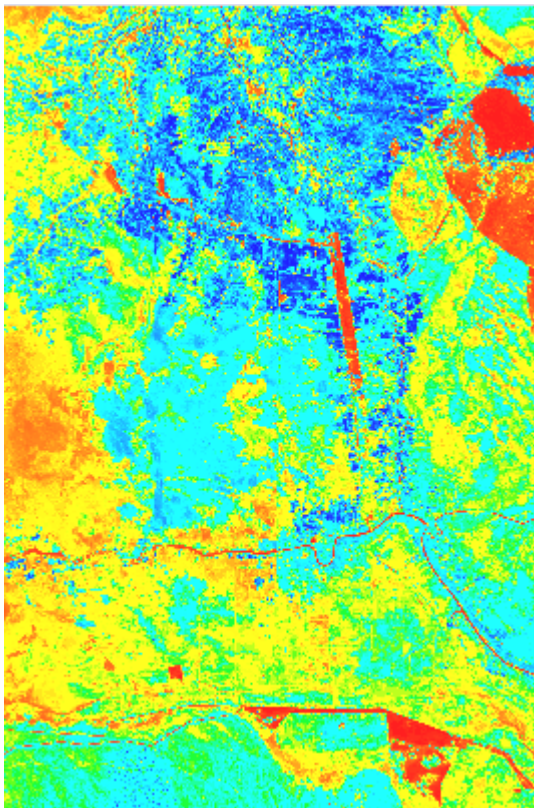
Its clear from NDVI images that the bright areas (that represent vegetation) for Al-Hawizah, Al-Hammar, and Central marshes in 1973 and 1990 images, converted to dark areas in 2000, 2003 and 2004 due to desiccation of these marshes. In NDVI image for Landsat ETM+ (26/3/2000) bright areas absent in Al-Hammar marsh and Central marsh. In NDVI image for Landsat ETM+(6/5/2003) small part of vegetation marsh (bright area) began reflooding in Al-Hawizah and Al-Hammar marshes. In NDVI image for image Landsat ETM+ (2/2/2004) small part of vegetation began reflooding in Al- Central marsh as shown in figure (4-16, E). Figure (4-17) shows false color NDVI images; the areas of high NDVI value appear in blue color (marsh vegetation and agriculture) and low vegetation (low value) appears in red color. It is clear that water and wet area in red or yellow color and barren land in green or yellow color.



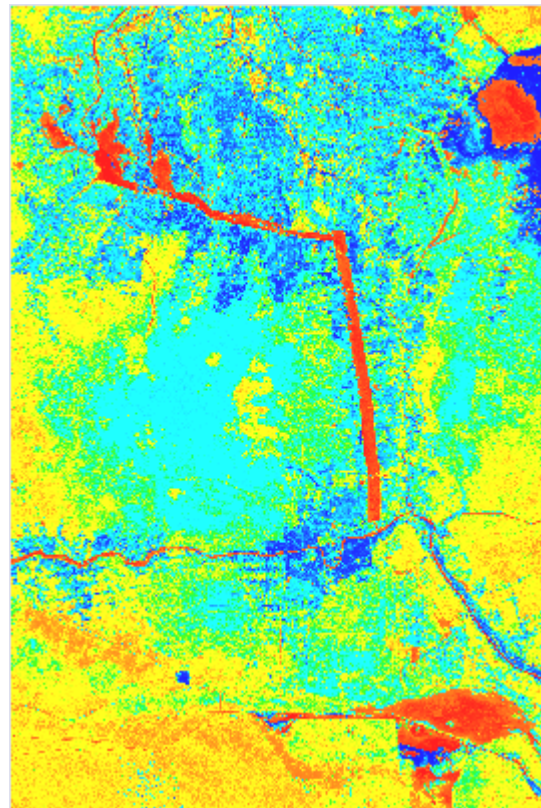
A- False color for NDVI image 1973



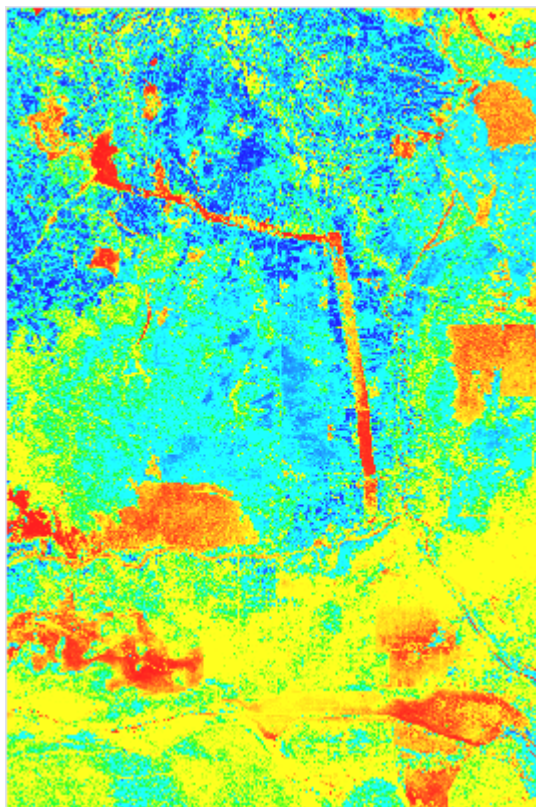
*B- false color for NDVI image
(7/9/1990)*



*C- false color for NDVI image
(26/3/2000)*



*D- false color for NDVI image
(6/5/2003)*



E- false color for NDVI image (2/2/2004)

Figure (4-17) show NDVI images with false color

Table (4-5) Average NDVI for land use classes.

Class Name	1973		1990		2000		2003		2004	
	NDVI value	NDVI scaled	NDVI value	NDVI scaled	NDVI value	NDVI scaled	NDVI value	NDVI scaled	NDVI value	NDVI scaled
Water	-0.73	34	-0.56	56	-0.48	66	-0.41	75	-0.077	118
Wet land	0.04	133	0.149	146.12	-0.039	122.57	-0.135	110.25	0.095	139.6
Barren	0.07	136	0.180	150.60	0.034	131.79	-0.121	112.12	0.095	140.68
Marsh veg.	0.521	194	0.510	192.56	0.226	156.36	0.055	134.56	0.103	161.42
Agriculture	0.611	205	0.637	208.68	0.392	177.48	0.247	159.04	0.469	187.34

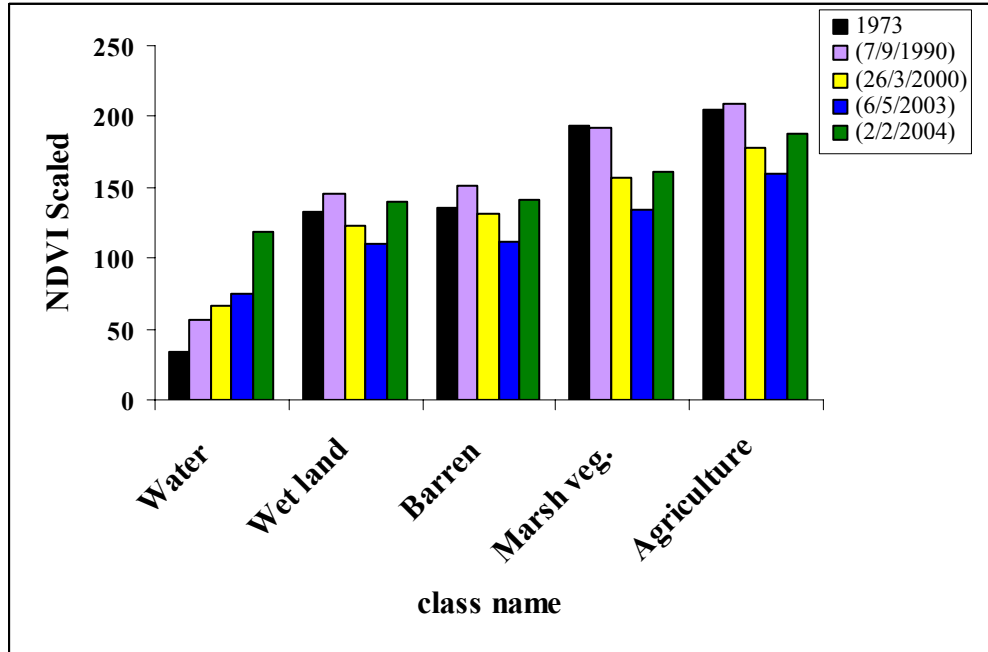


Figure (4-18) average NDVI for land use classes

According to table (4-5) and figure (4-18) which show relation between average NDVI and land use classes, the classes that have vegetation cover show high NDVI value (such as marsh vegetation and agriculture). Water and wet soil have lower NDVI than other land classes.

4-5 Surface Radiant Temperature:

After producing images enhancement for Landsat thermal images, surface temperature was calculated to understand the impacts land use/cover change on surface radiant temperature. The surface temperatures were derived from the thermal band radiance values of the sensor (TM and ETM+). The digital numbers were transformed into radiance using equation (3-9) which can be expressed as

$$L_{\lambda} = \left\{ \frac{L_{\text{MAX}} - L_{\text{MIN}}}{255} \right\} * \text{DN} + L_{\text{MIN}}$$

Where L_{λ} is the spectral radiance, L_{MIN} and L_{MAX} are spectral radiances for each band at digital numbers 0 and 255 respectively. For Landsat5 TM, L_{MIN} and L_{MAX} is 0.124 and 1.560 ($\text{mW.cm}^{-2}.\text{sr}^{-1}.\mu\text{m}^{-1}$) respectively. For Landsat 7 ETM+ the following values are given:

High gain : $L_{\text{MIN}}=3.2$ $L_{\text{MAX}}=12.65 \text{ W.m}^{-2}.\text{sr}^{-1}.\mu\text{m}^{-1}$

The spectral radiance was converted into surface radiant temperature values by using the relationship: [16]

$$T = \frac{K_2}{\ln[(K_1/L_{\lambda}) + 1]}$$

Where K_1 , K_2 are calibration constants, for Landsat 5 TM constants

$$K_1 = 60.776 \text{ mW.cm}^{-2}.\text{sr}^{-1}.\mu\text{m}^{-1}$$

$$K_2 = 1260.56 \text{ K}$$

For Landsat 7 ETM+

$$K_1 = 666.09 \text{ W.m}^{-2}.\text{sr}^{-1}.\mu\text{m}^{-1}$$

$$K_2 = 1282.71 \text{ K}$$

Figure (4-19) show example of surface temperature extracted Landsat TM image (7/9/1990). Its appearance from figure cursor is pointed to file pixel (the actual pixel value from the data, [33]). This pixel value is converted to radiance, then converted to surface temperature by using equations (3-11), (3-12) (see chapter three).

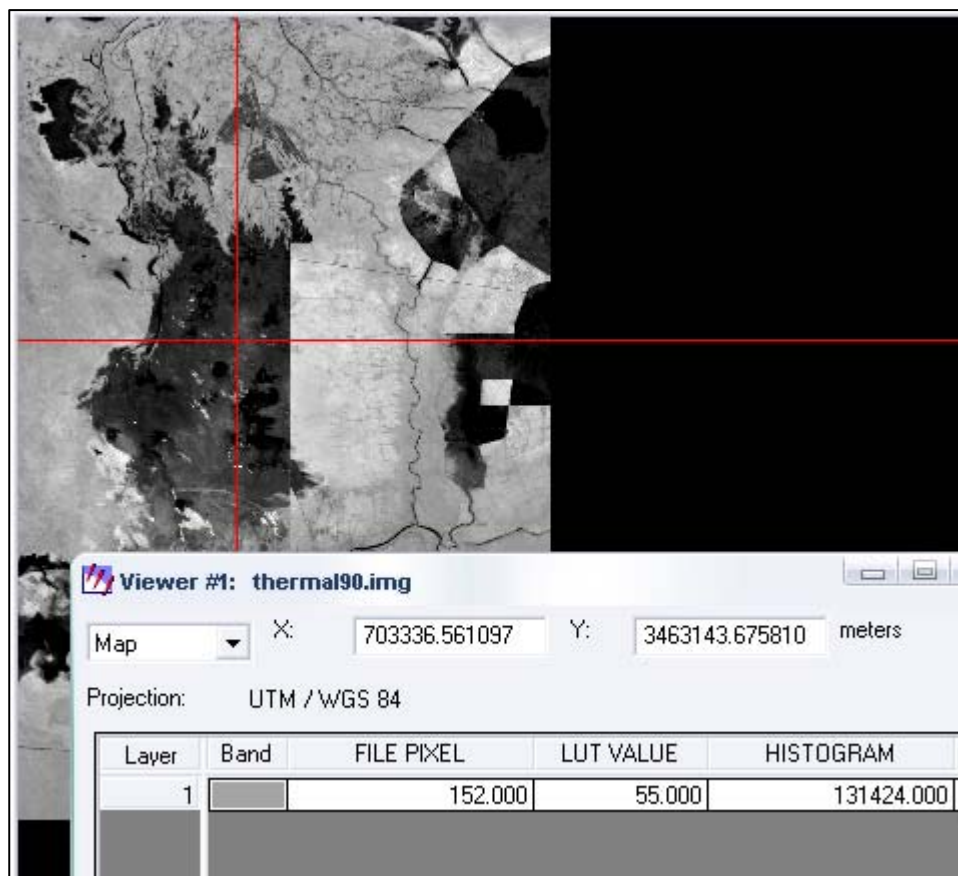
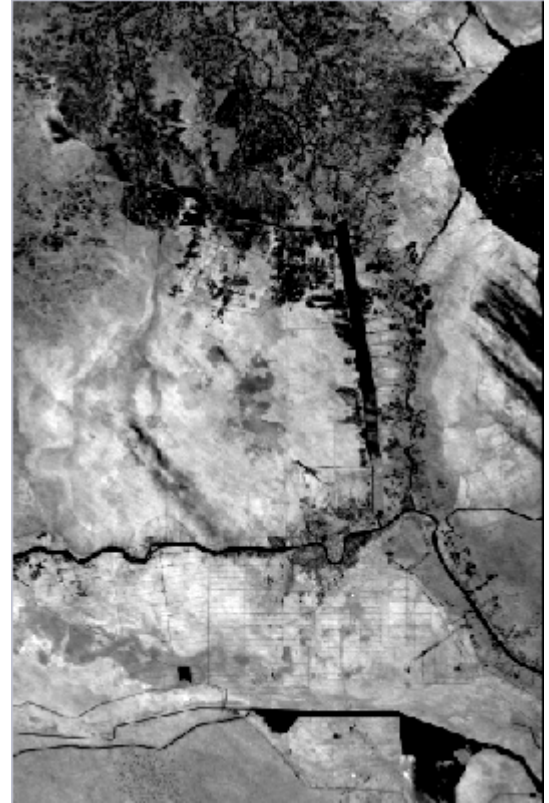


Figure (4-19) Show calculate surface temperature

Surface temperatures are calculated for Landsat TM 1990 and Landsat ETM+ 2000, 2003 images that represent study area as shown in figure (4-20). This figure shows that the dark areas have low surface temperature and bright areas have high surface temperature.



*A- Thermal image for image
Landsat TM (7/9/1990)*



*B- Thermal image for image
Landsat ETM+ (26/3/2000)*

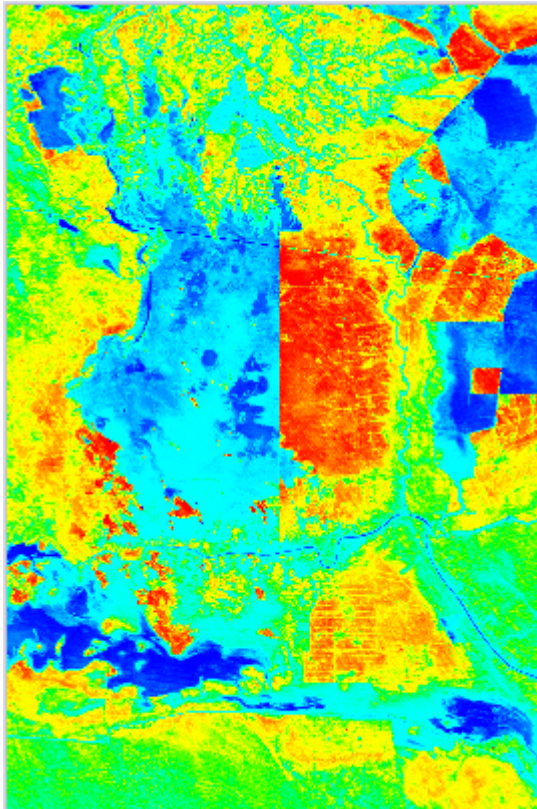


*C- Thermal image for image
Landsat ETM+(6/5/2003)*

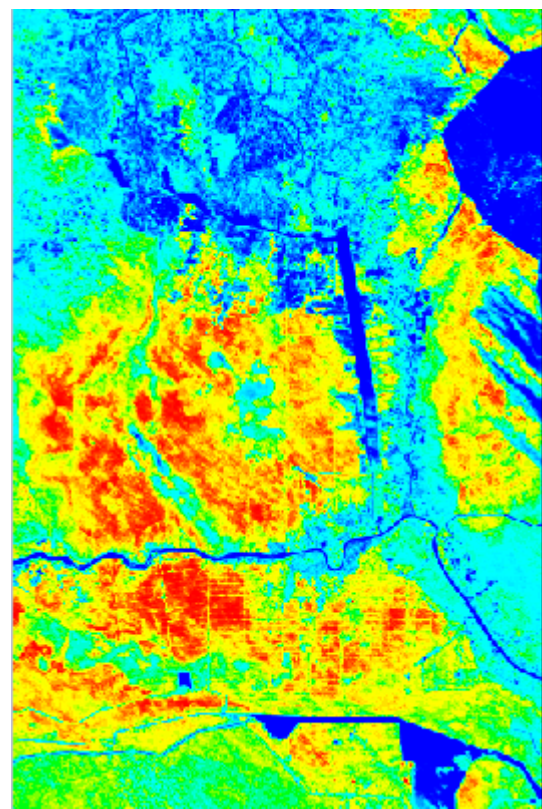


*D- Thermal image for image
Landsat ETM+ (2/2/2004)*

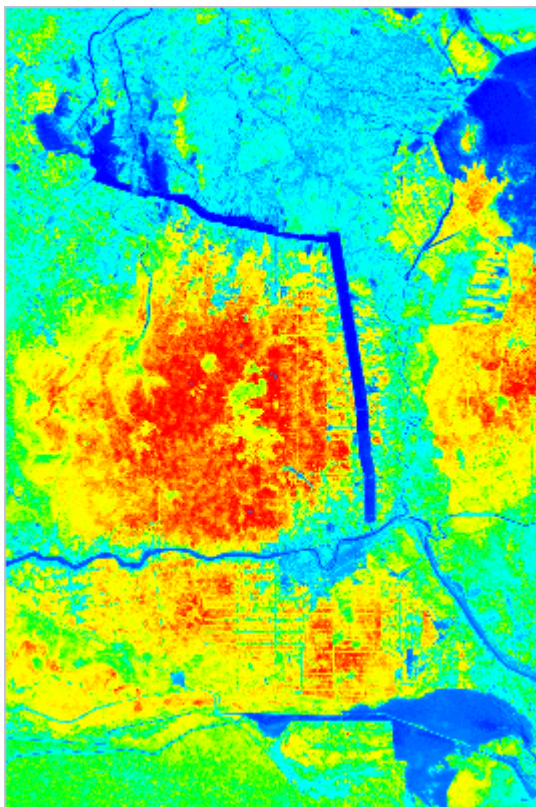
Figure (4-20) Thermal images for study area



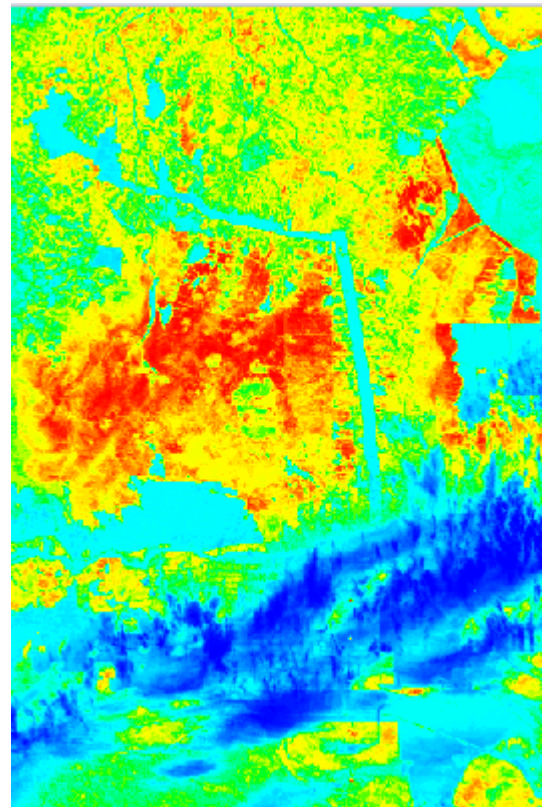
*A-Thermal image for (7/9/1990)
with false color*



*B- Thermal image for (26/3/2000)
with false color*



*C -Thermal image for (6/5/2003)
with false color*



*D- Thermal image for (2/2/2004)
with false color*

Figure (4-21) Thermal images with false color

Figure (4-21) shows thermal images with false color, low temperature in blue color such as water, and vegetation (agriculture, vegetation marsh) and high temperature in red or yellow color such as wet area and barren area. Table (4-6) and figure (4-22) illustrate relation between surface temperature and land use class.

Table (4-6) Average surface temperature for land use classes

Class name	(7/9/1990)	(26/3/2000)	(6/5/2003)	(2/2/2004)
	Average temp. °C	Average temp. °C	Average temp. °C	Average temp. °C
Water	22.43	10.47	17.92	9.95
Wet land	46.79	24.69	32.85	16.44
Barren land	41.88	22.63	31.46	14.03
Marsh vegetation	34.51	20.54	28.7	12.90
agriculture	31.36	18.60	24.50	12.85

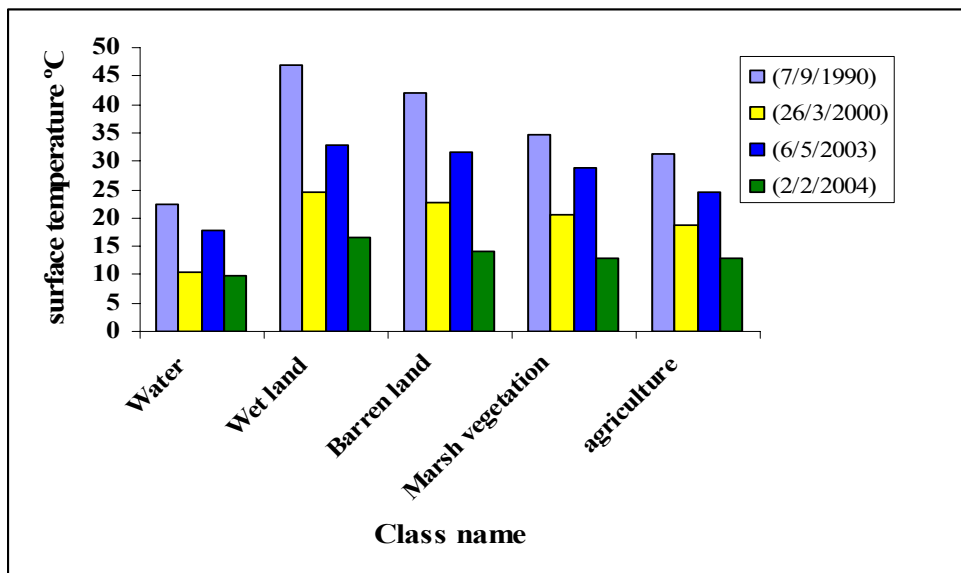


Figure (4-22) Average temperature for land use classes

It is clear from figure (4-22) and table (4-6) high temperature value in (7/9/1990), in spite of high vegetation cover, while (2/2/2004) shows the lowest temperature in the area. So we can conclude that air temperatures are effected on surface radiant temperature value, so that maximum air temperature in September and minimum in February month.

4-6 Correlation analysis of surface temperature and NDVI:

NDVI is negative correlation with surface temperature [16]. The relation between surface temperature and NVDI was investigated for each land cover type through correlation analysis (pixel by pixel). Table (4-7) show the correlation analysis between surface temperature and NDVI for the study years. It is clear from the table (4-7) the surface temperature values tend to negatively correlate with NDVI values for all years and land cover types.

Table (4-7) Correlation analysis of temporal surface temperature and NDVI

years	Correlation equation	R ²
(7/9/1990)	$y = -0.2206x + 77.105$	0.9283
(26/3/2000)	$y = -0.1059x + 37.18$	0.9621
(6/5/2003)	$y = -0.154x + 49.235$	0.9488
(2/2/2004)	$y = -0.0641x + 23.958$	0.6495

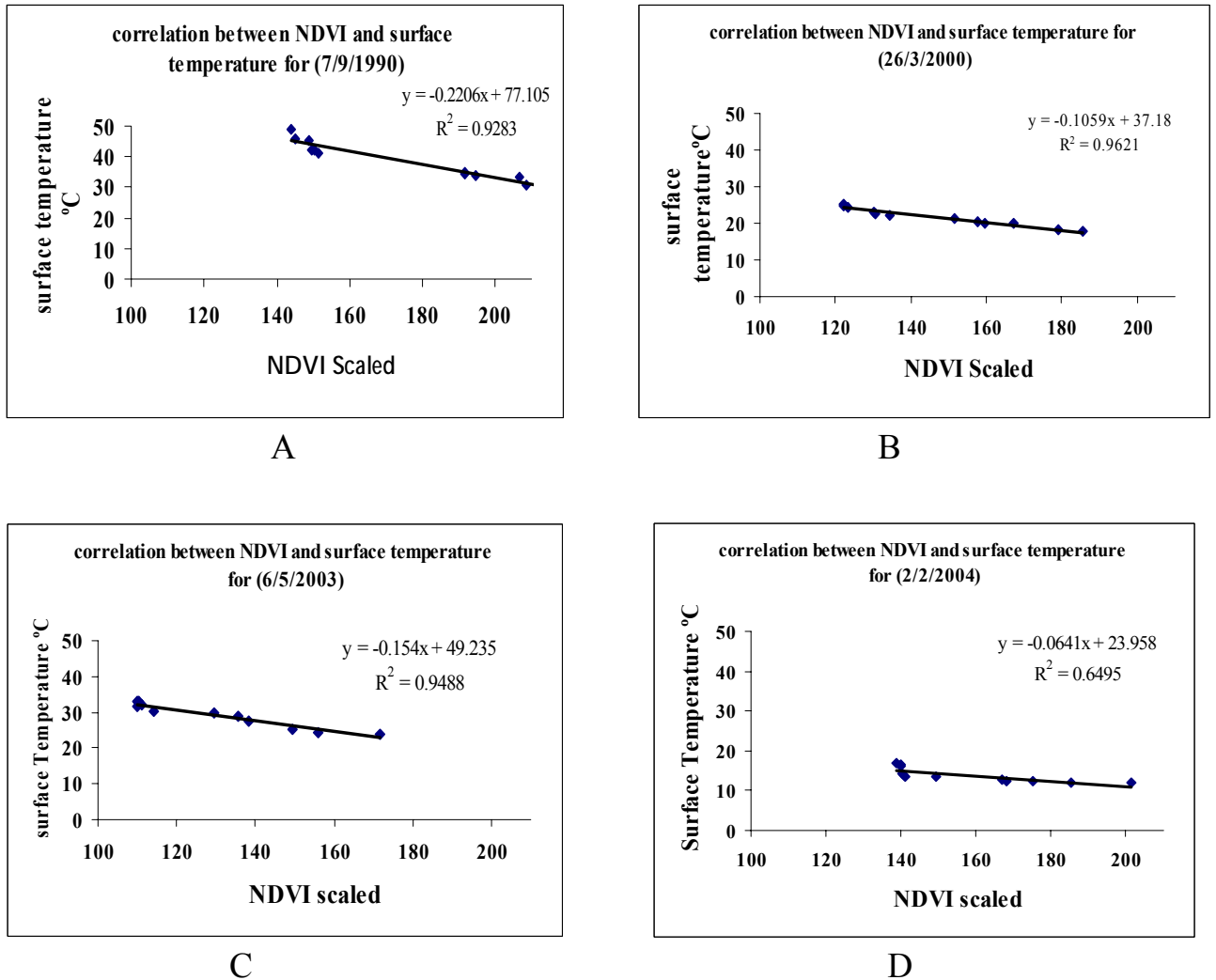


Figure (4-23) show correlation between NDVI and surface temperature

It is clear from figure (4-23) agriculture cover types is located in the right lower corner of the figure, barren and marsh vegetation in the centre of the figure, while wet land is located in upper left corner of the figure.

The results revealed that agriculture and marsh vegetation lands have lowest surface temperature and highest NDVI, this due to in fact, the increase vegetation reduce in surface temperature.

CHAPTER FIVE
Conclusions and Recommendations

5-1 Conclusions:

1. Environmental changes in Iraqi marsh during the period 1973-2004, effects on vegetation and water (ecosystem). Clear changes have occurred in marsh draining, reducing vegetation and water with increasing in barren and wet lands.
2. The results show that marsh vegetation decreased about 30.10% in 1990, 40% in 2000, 43.2% in 2003, 30.10% in 2004; comparable with 1973. While wet area increase about 23.90%, 23.00%, 36.50% , 23.70% for 1990, 2000, 2003 and 2004 respectively comparable with 1973. Barren area increase about (1.20 -26.00)% during the period 1990-2000, after that decrease when reflooding marshes.
3. The results of the correlation analysis between land surface temperature and NDVI show negative correlation for all land use types. The analysis indicated that agriculture and marsh vegetation have the lowest surface temperature and high NDVI, but barren and wet land had highest surface temperature and low NDVI.
4. The main dominate factor on surface temperature value is air temperature. The results show that the higher surface temperature value in Sept. 1990 (high vegetation) than May 2003, March 2000 and February 2004.
5. It is possible to estimate surface temperature for 1973(where is no thermal band available) from NDVI value and correlation equation with another image. It was found NDVI for 1973 approximately

equal NDVI for 1990 therefore use correlation equation of 1990 to find surface temperature of 1973.

5-2 Recommendations:

1. Using multi-temporal and different resolution images for the same region and the same month with different years, for example (September 1990, September 2000....) to detect changes in the region.
2. Spectral reflectance and temperature signature reference prefer to be used in analysis and image interpretation.
3. Using different indices (for example soil adjust vegetation index (SAVI), bare soil index (BSI) and band ratios) to predict the relation between these indices and surface temperature of earth targets. This method will be quite used for the images with no thermal band.

REFERENCES

References:

1. Avery T.E., and Berlin G. L., (1992) "**Fundamental of Remote Sensing and Airphoto interpretation**", 5th ed., Prentice- Hall, Inc.
2. Riadh K.A., (2005) '**Change Detection of Environmental system using satellite images in Shatt AL-Arab region**', M.SC. Thesis, University of Technology, Iraq.
3. Ali K.S.,(2006) "**Remote Sensing and GIS for Aquatic Environment of Iraqi Marshes**", M.SC. Thesis, University of Technology, Iraq.
4. Water and land Resources (1998), available on line at <http://dnr.metroke.gov/wlr>.
5. U.S. Environmental Protection Agency (2005), available on line at: <http://www.epa.gov/owow/wetland/types/marsh>
6. Earth shots: Satellite Images of Environmental change :Iraq-Kuwait, (2007), available on line at <http://edcwww.cr.usgs.gov/earthshots/slow/Iraq/Iraq>
7. NASA earth observatory "Vanishing Marshes of Mesopotamia", Report UNEP, available on line: http://earthobservatory.nasa.gov/newsroom/newimages/images.php3?img_id=5112
8. Iraq-Marsh Arabs, available on line at: <http://homepage.mac.com/weblink/Iraq/p05-MarshArab.htm>
9. UNEP report (2005),"Iraqi Marshlands Observation System", available on line at: <http://imos.grid.unep.ch>
10. Back grounders(2003), "Iraqi Government Assault on the Marsh Arabs", available on line at: www.hrw.org/backgrounders/mana/MarshArabs1.htm

11. Partow H. , (2001), "The Mesopotamian Marshlands : Demise of an Ecosystem " ,report UNEP available on line at:
<http://earthobservatory.nasa.gov/newsroom/NewImages/Meso2.pdf>
12. James W.B., (2002), "The Tigris – Euphrates Marshlands", available on line at:
<http://www.jameswbell.com/a007tigriseuphratesmarshlands.html>
13. UNEP study (2002), "Mesopotamian Marshes 1973" available on line at :
http://www.ncciraq.org/IMG/pdf_UNEP_deskstudy_on_environment_in_Iraq_part2.B.pdf
14. Marine Science Center, (2005), "The Ecology of the Marshland of Iraq", Train Course, Basrah University.
15. Iraq-weather maps , available on line at
<http://www.wunderground.com/newspaper/Iraqi/index.php>.
16. Weng Q.,(2001)" A remote Sensing –GIS evaluation of urban expansion and its impact on surface temperature in the Zhujiang Delta, Chin", international journal of remote sensing, VO.22,NO.10,P.1999-2014
17. Ping C., Soo C.L. and Leong K.K., (2001)" Dependence of urban temperature elevation land cover types" National University of Singapore.
18. Zhou L.,et al, (2003)"Relation between internal Variation in Satellite measures of northern forest greenness and Climate between 1982 and 1992",Journal,Geoph., Res.,108(D1),4004,doi:10.1029/2002JD000250
19. Akkartat A., Turudu O. and Erbek F.S.,(2004) "Analysis of changes in vegetation Biomass using multi-temporal and multi-sensor Satellite data", Stanbul Technical University, available on line at:
www.isprs.org/istanbul2004/f/papers/946.pdf.

20. Andy Y.K. and Christopher s., (2004)" Comparative analysis of thermal environments in New York city and Kuwait city" Sultan Qaboos University, available on line at:
www.isprs.org/commission8/workshop-urban/kwarteng.pdf.
21. UNEP (2005),"Iraqi Marshlands monitoring Reflooding and vegetation change", available on line at :
<http://imos.grid.unep.ch/unloads/050902.pdf>
22. Myung H.J., and et al (2006) " The extraction method of surface temperature in agriculture area using Satellite Remote Sensing and GIS", Kyungil University, available on line at:
www.gisdevelopment.net/application/agriculture/overview/agrio012.htm-19k.
23. Aseel A. S., (2006) " Application of Remote Sensing and GIS Technique for soil description of Al-Hammar Marsh" , M.SC. Thesis, university of Technology, Iraq.
24. Emzahim A. A., " Environmental Evaluation of Marshes zone using Remote Sensing and GIS Technique ", PHD. Thesis , unvirsiy of Technology, Iraq.
25. Civco D.J, (2004), "Fundamental of Remote Sensing ", Canada Center for Remote Sensing , available of line at:
www.citiesalliance.org/doc/resoures/upgrading/urban-expansion/3.pdf
26. Canada Center for Remote sensing , (2004)" Fundamentals of remote sensing ", available on line at:
<http://www.ccrs.nrcan.gc.ca/ccrs/learn/tutorials/fandom/chapter1>.
27. Jensen J.R., (2000),"Remote sensing of the environment: An earth resource perspective", Upper Saddle River., NJ: Prentice Hall
28. Gibson P.J. and Power C.H., (2000)," Introduction remote sensing principles and concepts", Routledge, Taylor and Francis Group, London.

29. Steven M.D., Raymond S., Maarten Z., Elisabeth A., (2005) "Remote Sensing a tool for Environmental Observation" Utrecht University, the Netherlands.
30. Lillesand T.M. and Kiefer R.W., (2000) "Remote sensing and image interpretation", 4th ed., John Wiley and Sons, New York.
31. Curran P.J., (1985), "Principles of remote sensing ", Longman, London.
32. Swain P.H. and Davis S.M. (1978), "Remote Sensing the Quantitative Approach" Mc Graw, Hill Inc.
33. ERDAS Imaging Field Guide ,(1998), Inc, Atlanta, Georgia.
34. Barry S.S, (1980), "Remote Sensing in Geology", image interpretation", John Wiley and sons, New York.
35. Jackson R.D., Moran M.S. (1987), "Field Calibration of reference reflectance panels", Arizona, J22, p.145-145.
36. Ala S.H., (2003) "Digital Techniques for Land use and land cover change detection", thesis, Baghdad University, Iraq.
37. Aubrey W., (2002) "The integration of remote sensing data into geographic information systems", George Mason University
38. Niblack W., "Application to digital image processing " pp(129-137), Prentice-Hall ,International .
39. Ramsey D.R., "Geometric correction of remotely sensed data" Remote Sensing Core Curriculum, Volume 3, Module 5.2., Accessed: Nov.7,2002, Available on line at <http://www.cla.sc.edu/geog/rslab/rssc/>.
40. Campbell J.B., (1996) "Introduction to remote sensing", 2nd ed., Taylor and Francis, London.
41. Alyaa H.A., (2002), "Classification of Digital Satellite Image using Selective Bands and Principles Component Analysis", M.SC., thesis, AL-Nahrain University, Iraq.

42. Win H.B., Ambro S.M., Ben G.H.,(2004), "Principles of remote sensing", ITC, Enschede, The Netherlands
43. Japan association of remote sensing ,(1996).
44. Mustafa N.H. , (2006), "Urban Growth for Baghdad city using Remote Sensing and GIS Techniques", M.SC., thesis, University of Technology, Iraq.
45. Sabins F.F. ,(1978) "Remote Sensing Principle and interpretation", 1st ed., W.H. Freeman and company.

الملخص:

تعتبر الاهوار من اكبر المسطحات المائية في العالم وان اهوار جنوب العراق من أهم هذه المسطحات ومن أغنى مناطق العالم بالحياة البرية متمثلة بالبحيرات الضحلة الكثيفة الأعشاب والمغطاة بالقصب والبردي .

تعرضت هذه المنطقة إلي عدة تغيرات سواء كانت هذه التغيرات طبيعية أو اصطناعية، وأثرت التغيرات الحاصلة على النظام البيئي لمنطقة الاهوار (الغطاء الارضي ، النباتي والبيئة المائية).

يهدف البحث الحالي الى كشف التغيرات البيئية الحاصلة في منطقة الاهوار للفترة (1973-2004) باستخدام صور لاندسات متعددة الاطراف وبتواريخ مختلفة وباستخدام التقنيات الرقمية للصور. تتضمن هذه التقنيات إجراء عملية المؤزائيك لبعض الصور وذلك للحصول على منطقة الدراسة ، التصحيح الهندسي، التحسينات لبعض الصور الحرارية ، إجراء عملية التصنيف غير الموجه (unsupervised) باستخدام طريقة(Isodata) والموجه (supervised) باستخدام طريقة (maximum Likelihood) ، حساب دليل الخضرة NDVI لصور (1973، 1990، 2000، 2003، 2004) ،حساب درجات الحرارة لصور (1990، 2000، 2003 ، 2004) .

لوحظ من خلال النتائج وصور لاندسات المستخدمة إن منطقة الاهوار قلت فيها مناطق الغطاء النباتي والمياه خلال الفترة 1973-2003 وثم نلاحظ رجوع المياه في سنة 2003. أيضا النتائج بينت إن NDVI يعد مؤشر جيد لوجود المساحات الخضراء حيث إن وجود الغطاء النباتي يقلل من درجات الحرارة في المنطقة لذلك فان العلاقة بين NDVI ودرجات الحرارة علاقة عكسية حيث ان زيادة المساحات الخضراء يقلل الضرر البيئي .



جمهورية العراق
وزارة التعليم العالي والبحث العلمي
جامعة النهرين/ كلية العلوم
قسم الفيزياء

متابعة تحليل التغيرات البيئية لمنطقة الاهوار باستخدام صور لاندسات

رسالة مقدمة الى كلية العلوم في جامعة النهرين كجزء من متطلبات نيل
شهادة الماجستير في علوم الفيزياء

من قبل
عشتار حسين ناصر
(بكالوريوس ٢٠٠٤)

بإشراف
د. صلاح عبد الحميد صالح

١٤٢٨ هـ
2007 م

شوال
تشرين الثاني